

Evaluating the Importance of Initial Conditions for
Antarctic Sea Ice Seasonal Predictability with a
Fully Coupled Forecast Model

Elio Campitelli^{1,2*}, Ariaan Purich^{1,2}, Julie Arblaster^{1,2},
Eun-Pa Lim³, Matthew C. Wheeler³, Phillip Reid³

¹School of Earth, Atmosphere and Environment, Monash University,
Australia.,

²Securing Antarctica's Environmental Future, Monash University,
Australia.

³Research, Bureau of Meteorology, Australia.

*Corresponding author(s). E-mail(s): elio.campitelli@monash.edu;

Abstract

Accurate Antarctic sea-ice forecasts are crucial for climate monitoring and operational planning, yet they remain challenging due to model biases and complex ice-ocean-atmosphere interactions. The two versions of the Australian Bureau of Meteorology's ACCESS seasonal forecast system, ACCESS-S1 and ACCESS-S2, use identical model configuration and differ only in their initial conditions; primarily in that ACCESS-S2 does not assimilate sea-ice observations, whereas ACCESS-S1 does.

This provides an convenient opportunistic experiment to assess the role of initial conditions on Antarctic sea-ice forecasts using more than 20 years of fully coupled simulations with two 9-member ensembles. Our analysis reveals that both systems experience an extended melt season and delayed growth phase compared with observations. This leads to a significant negative sea-ice extent bias, which is corrected only in ACCESS-S1 by the data assimilation system. The impact of

047 the differing initial conditions on forecast errors varies dramatically by season:
048 summer and autumn initial conditions (January-April) provide predictive skill for
049 up to three months, with February initial conditions being particularly crucial.
050 In contrast, winter forecasts of the two systems are statistically indistinguish-
051 able after only two weeks. Regional analysis of forecast skill suggests that this
052 winter predictability barrier is most dramatic over East Antarctica, where even
053 ACCESS-S1 shows negative skill. These findings highlight the critical importance
054 of comprehensive year-round sampling in predictability studies and suggest that
055 operational sea-ice data assimilation efforts should prioritize the summer-autumn
056 period when initial conditions have maximum impact on forecast skill.

057 **Keywords:** sea ice, seasonal predictability, initial conditions, forecasting

063 Introduction

064
065
066 Accurately modelling Antarctic sea ice is essential for understanding processes and
067 improving climate projections to inform adaptation strategies. Accurate seasonal to
068 sub-seasonal forecasts are also crucial for operation contingency planning in and
069 around the Antarctic continent, including scientific missions, fisheries, and tourism^{1;2}.
070
071 Improvements in modelled sea-ice might also help improve weather forecasts over and
072 away from sea-ice regions^{3–5}.

073
074
075
076 However, progress in Antarctic sea-ice forecasting system has lagged behind Arctic
077 sea-ice forecasts due to model biases, and inherent large variability and complexity^{6;7}.
078
079 Dynamical seasonal forecasts of summer Antarctic sea ice have been shown to perform
080 worse than relatively simpler statistical methods⁸ and machine learning approaches (e.g.
081 Dong et al.⁹, Lin et al.¹⁰), which also underscores the need for better understanding
082 and physical modelling of sea-ice dynamics, and drivers of its variability.

083
084
085
086 Good initial conditions are generally required for a good forecast, however, it is not
087 entirely known to what extent accurate sea-ice initial conditions affect the quality of
088 the forecast and at what timescales. Exploring seasonal predictions of Arctic sea ice,
089 Guemas et al.¹¹ found that sea-ice initial conditions are important in autumn to predict

summer sea ice, but the impact wasn't as dramatic when predicting winter sea ice. Day et al.¹² also found seasonally-varying differences in the effect of initialisation, noting that accurate Arctic sea-ice thickness leads to improved sea-ice forecasts initialised in July but not when initialised in January.

For the Antarctic, Holland et al.¹³ studied the initial-value predictability of Antarctic sea ice in a perfect model study using the CCSM3 model. They found that sea-ice and ocean initial conditions provide predictive information to forecast sea-ice edge location several months in advance and that some predictability is retained for up to two years thanks to ocean heat content anomalies that are advected eastward. This is in contrast with Marchi et al.¹⁴, who ran perfect model experiments to argue that uncertainty in the predicted atmospheric state and evolution is the main driver of uncertainty in Antarctic sea-ice extent prediction on seasonal timescales, with sea-ice and ocean initial conditions having lesser importance. More recently, Morioka et al.¹⁵ studied decadal forecasts of Antarctic sea ice and found that initialising ocean and sea ice improved the correlation between simulated and observed sea-ice concentration evolution in the Amundsen–Bellingshausen Sea. It is hard to compare these studies since they are based on forecasts initialised at different times of the year and different frameworks: Holland et al.¹³ ran 20 ensemble members initialised on the 1st of January of a particular year, Marchi et al.¹⁴ ran forecasts from the 1st of March and 1st of September, and Morioka et al.¹⁵ ran forecasts only from the 1st of March. Marchi et al.¹⁴ also used a coupled ocean–sea-ice model instead of a fully coupled model like Holland et al.¹³ did. Morioka et al.¹⁵ used observed sea-ice initial conditions and compared with observations, while Marchi et al.¹⁴ and Holland et al.¹³ were perfect model studies.

In October 2021 the Australian Bureau of Meteorology (BoM) upgraded the Australian Community Climate and Earth System Simulator – Seasonal (ACCESS-S) from version S1 to S2. While the base model remained the same, the change in version was focused on using ocean, sea-ice and land initial conditions generated by the BoM instead of

139 depending on the UK Met Office. Crucially, compared to ACCESS-S1, ACCESS-S2
140 does not assimilate sea-ice observations, so sea ice is only affected by the ocean and
141 atmospheric data assimilation via the coupled integration.
142

144 Since model configuration is identical between ACCESS-S1 and ACCESS-S2, they
145 form a sort of “opportunistic experiment” where the same forecasting model was run
146 over a long period of time with multiple ensemble forecasts initialised throughout the
147 year, with the only difference being the initial conditions. This provides an opportunity
148 to test the effect of sea-ice initial conditions on the forecast of sea-ice concentrations
149 and the climate.
150

154 In this study we compare sea-ice hindcasts produced by ACCESS-S1 and ACCESS-S2.
155 We focus on seasonality of errors and biases and the effect of the data assimilation
156 system. This comparison will inform future work with the prediction system as a
157 research tool to better understand the dynamics and variability of the Antarctic sea
158 ice and its impacts on the climate system as well as to explore the potential of using
159 its sea-ice forecasts for decision-making. The work will also serve as a benchmark for
160 future prediction systems to attempt to improve upon.
161

168 **Data and methods**

172 **ACCESS-S2**

174 ACCESS-S2¹⁶ is the Bureau of Meteorology’s seasonal forecast system which became
175 operational in October 2021, replacing the ACCESS-S1 system¹⁷. The model com-
176 ponents of both ACCESS-S2 and ACCESS-S1 are identical with the same numbers
177 of levels and resolution. They consist of the Global Atmosphere 6.0 (GA6)^{18;19}, the
178 Unified Model’s Global Land 6.0^{19;20}, NEMO Global Ocean 5.0^{21;22} and Global Sea
179 Ice 6.0 [CICE; Rae et al. ²³]. The atmosphere has a N216 horizontal resolution (~60 km
180
181
182
183
184

in the mid-latitudes) with 85 vertical levels. The land model uses the same horizontal grid as the atmosphere with four soil levels. The ocean component has a nominal horizontal resolution of $1/4^\circ$ with 75 vertical levels. The sea-ice component, based on CICE version 4.1, has the same resolution as the ocean component and five sea-ice thickness categories as well as an open water category. 185
186
187
188
189
190
191
192
193
194
195
196
197
198
199
200
201
202
203
204
205
206
207
208
209
210
211
212
213
214
215
216
217
218
219
220
221
222
223
224
225
226
227
228
229
230

Both systems take atmospheric initial conditions derived from ERA-interim²⁴ for their hindcasts. The main difference between the hindcasts of the two systems are the ocean and sea-ice initial conditions. ACCESS-S1's ocean and sea-ice initial conditions come from the Met Office FOAM system, which uses a multivariate, incremental three-dimensional variational (3D-Var), first-guess-at-appropriate-time (FGAT) data assimilation scheme²⁵ and assimilates sea surface temperature (SST), sea surface height (SSH), in situ temperature and salinity profiles, and satellite observations of sea-ice concentration using the EUMETSAT OSISAF product described in the next section. ACCESS-S2, on the other hand, is initialised from ocean conditions generated by the BoM weakly coupled ensemble data assimilation scheme described in Wedd et al.¹⁶. This scheme uses an optimal interpolation method and assimilates temperature and salinity profiles from EN4²⁶. SSTs are nudged to Reynolds OISSTv2.1²⁷ in areas where SSTs are over 0°C and Sea Surface Salinity is weakly nudged to the World Ocean Atlas 2013 climatology²⁸.

Of most relevance for this work, sea-ice concentrations are not assimilated in ACCESS-S2. Assimilation cycles are performed daily. The coupled model runs for 24 hours initialised from the previous cycle. Then the restart file fields of the ocean component are used as first guess in the data assimilation cycle and the innovations are used to build the next ocean initial conditions for the following cycle. The atmosphere fields from that daily integration are not used and instead the model atmosphere is initialised using ERA-Interim. The sea-ice initial conditions for the next cycle are the unaltered output of the previous daily integration. Then the cycle starts again and the coupled

231 model runs for another 24 hours. During this integration the sea-ice component is
232 affected by the ocean innovations and the new atmosphere initial conditions via the
233 coupler.
235

236 The ACCESS-S1 hindcast set is made up of nine members created by perturbing the
237 atmospheric fields only with a random field perturbation¹⁷ and runs for 217 days for
238 the period 1990–2012 initialised at the first of every month. The ACCESS-S2 hindcast
239 set used in this study runs for the period 1981–2018. Each hindcast consists of nine
240 ensemble members built from three consecutive three-member forecasts created in the
241 same manner as ACCESS-S1 members initialised at the first of every month and the
242 two previous days and run for 279 days. We analyse the ensemble mean hindcasts
243 unless otherwise specified.
249

250 Anomalies for each hindcast set are taken with respect to their own climatology specific
251 to each initialisation date and forecast lead time, for the period 1990–2012. This serves
252 as a first-order correction of model bias and drift. For monthly means, we define “0
253 lead time months” as the monthly mean forecast of the same month of initialisation.
256

257 Besides sea-ice concentration, we also analyse mean sea-ice thickness, which we compute
258 as total sea-ice volume divided by total sea-ice area.
260

261
262 **Verification datasets**
263

264
265 For verification we use satellite-derived sea-ice concentration, which estimates the
266 proportion of each grid area that is covered with ice. Datasets derived using different
267 algorithms and satellite platforms, each have their own biases and uncertainties.
268 Estimates of inter-product uncertainty of sea-ice extent (SIE, defined here as the total
269 region of the Southern Ocean with at least 15% sea-ice cover) is of the order of 0.5
270 million km^2 ²⁹. As will be shown below, this spread is minimal compared with the
271
272
273
274
275
276

typical errors in the ACCESS-S2 and ACCESS-S1 forecasts, so the overall conclusions	277
of this study are independent of the verification dataset used.	278
	279
	280
We use NOAA/NSIDC's Climate Data Record V4 [CDR; Meier et al. ³⁰] as the pri-	281
mary sea-ice verification dataset. It takes the maximum value of the NASA Team ³¹	282
and NASA Bootstrap ³² sea-ice concentration products to reduce their low concen-	283
tration bias ^{30;33} . Both source algorithms use data from the Scanning Multichannel	284
Microwave Radiometer (SMMR) on the Nimbus-7 satellite and from the Special Sensor	285
Microwave/Imager (SSM/I) sensors on the Defense Meteorological Satellite Program's	286
(DMSP) -F8, -F11, and -F13 satellites. The data has a spatial resolution of 25 by 25	287
km and daily from November 1978 onwards.	288
	289
	290
	291
	292
	293
	294
The European Organisation for the Exploitation of Meteorological Satellites (EUMET-	295
SAT) Ocean and Sea Ice Satellite Application Facility [OSI; EUMETSAT Ocean and	296
Sea Ice Satellite Application Facility ³⁴] based on the SSMIS sensor is another satellite-	297
derived sea-ice concentration product. It is based on mostly the same sensors as the	298
NOAA CDR but computed independently using different algorithms. Figures pre-	299
pared with this dataset are provided in the supplementary material and do not differ	300
significantly from the ones prepared using CDR.	301
	302
	303
	304
	305
	306
	307
Error measures	308
	309
	310
For evaluation purposes, we use a series of measures. Sea-ice extent is defined as the	311
area of the ocean at least 15% covered by sea-ice. This threshold is motivated by	312
the limitations in satellite retrieval, which is increasingly unreliable for lower sea-ice	313
concentrations ³⁵ .	314
	315
	316
	317
Pan-Antarctic (net) sea-ice extent serves as a hemispheric measure of the amount of	318
sea ice, but it does not take into account the spatial distribution. A model could have	319
a relatively accurate extent of the net ice but with different regional distributions. To	320
	321
	322

323 account for location errors, we computed the Root Mean Squared Error (RMSE) of
324 grid-point sea-ice concentration anomalies.
325

326 We compute RMSE as the square root of the area-averaged squared differences between
327 grid-point forecasted and observed sea-ice concentration anomalies. We compute a
328 pan-Antarctic RMSE by averaging over the whole NOAA/NSIDC CDRV4 Southern
329 Hemisphere domain, and also a zonally-varying RMSE computed over 15 longitude
330 slices 24° wide around Antarctica.
331

332 All error measures were computed on the NOAA/NSIDC CDRV4 domain grid, to
333 which model output was bilinearly interpolated. Note that the ACCESS CICE model
334 grid has resolution between two and three times higher than NOAA/NSIDC CDRV4.
335

336 Forecasts errors are also compared with hypothetical forecasts based on the persistence
337 of anomalies and on climatology. The persistence forecast is generated by extending
338 the observed anomalies in time.
339

340 As a measure of forecast improvement over the hypothetical forecast, we use the skill
341 score³⁶, defined as
342

343

344

$$S = 1 - \frac{RMSE_f}{RMSE_r}$$

345

346 Where $RMSE_f$ is the RMSE of the forecast, $RMSE_r$ is the RMSE of the reference
347 forecast. Negative skill score indicates that the forecast is worse than the reference
348 forecast while positive values indicate an improvement. A perfect forecast, would have
349 zero RMSE and thus a skill score of 1.
350

351

352

353 **Computational procedures**

354

355

356 We performed all analysis in this paper using the R programming language³⁷, using
357 data.table³⁸ and metR³⁹ packages. Significant processing was performed using the
358

CDO command line operators⁴⁰. All graphics are made using ggplot2⁴¹. The paper was rendered using knitr and quarto^{42;43}.

Results and discussion

Bias

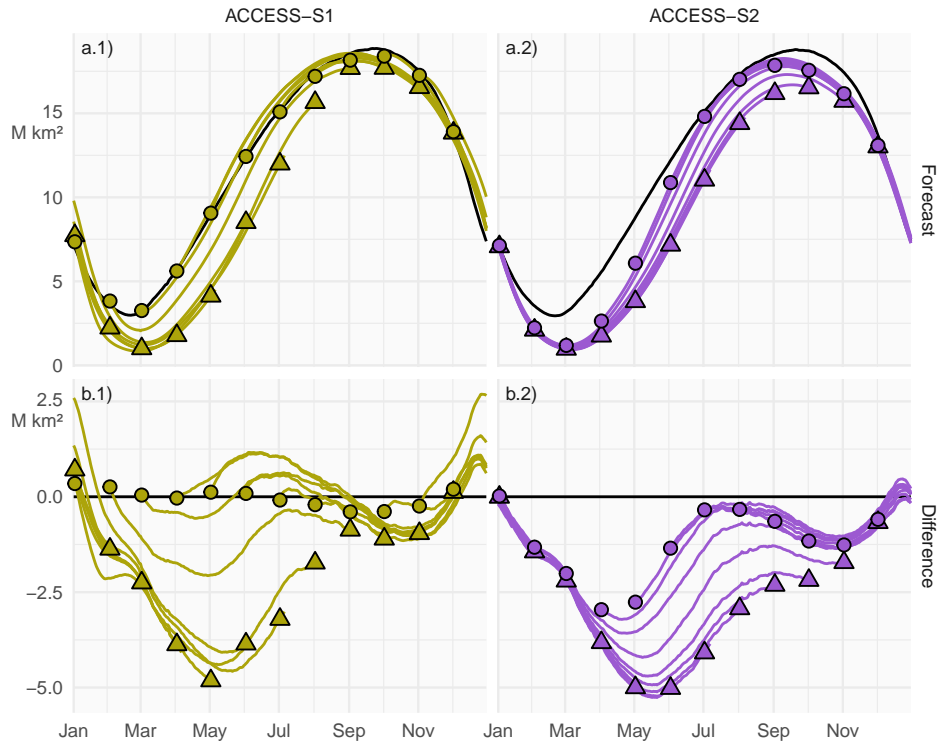


Figure 1: Row a: Pan-Antarctic mean sea-ice extent for all hindcasts initialised on the first of each calendar month for ACCESS-S1 (column 1; green) and ACCESS-S2 (column 2; purple). Observed mean sea-ice extent in each corresponding hindcast period is shown in black. Row b: Mean differences between the forecast and the observed values. Circles represent the initial conditions at the start of forecasts (i.e., the first of every month), and triangles represent the mean values at the end of forecasts (i.e., the longest possible lead time).

369
370
371
372
373
374
375
376
377
378
379
380
381
382
383
384
385
386
387
388
389
390
391
392
393
394
395
396
397
398
399
400
401
402
403
404
405
406
407
408
409
410
411
412
413
414

415 Figure 1 shows mean sea-ice extent of the ACCESS-S1 and ACCESS-S2 hindcasts
416 (row a) and their differences from mean sea-ice extent of NOAA/NSIDC CDRV4 (row
417 b). Mean extent at the first of every month is indicated with circles for the initial
418 conditions and with triangles for the longest lead time possible for each model (between
419 274 and 277 days for ACCESS-S2 and between 213 and 216 days for ACCESS-S1).
420 At this long lead time, information of the initial conditions is essentially lost and the
421 forecast reverts to each model's preferred equilibrium state.
422
423 ACCESS-S2 initial conditions (circles in Fig. 1 column 2) show an overall negative bias,
424 especially in the late summer-early autumn, while ACCESS-S1 initial conditions (circles
425 in Fig. 1 column 1) are very close to observations, as expected from the assimilation
426 of sea-ice observations to produce the initial conditions of ACCESS-S1. Both systems'
427 equilibrium states (triangles) show negative biases of sea-ice extent, particularly in the
428 growth phase of late-autumn and winter months. This is due primarily to the melt
429 season being longer than in observations and with faster melt between January and
430 March and the growing seasons being shorter with slower growth during March and
431 April. This is then followed by faster growth between May and July (Figure 2). Many
432 sea-ice models exhibit this systematic underestimation during the sea-ice minimum
433 and early freezing season⁸, which could indicate problems in the representation of
434 thermodynamics in the model⁶. It is also not surprising that both forecasting systems
435 converge to a similar equilibrium state because they share the same model formulation.
436
437 The difference between the initial conditions (circles) and the model equilibrium
438 state (triangles) can be mostly attributed to the effect of data assimilation, which
439 in ACCESS-S2 is due solely to the coupling of sea-ice with the atmosphere and the
440 ocean. From May to October, in ACCESS-S2 circles are closer to observations than
441 the triangles are, indicating that the information from the ocean and atmosphere data
442 assimilation is affecting sea ice and improving the initial conditions. During these
443 months, ACCESS-S1 can overestimate the sea-ice extent at short lead time. For the rest
444 of the year, ACCESS-S1 has a negative bias, while ACCESS-S2 has a positive bias.
445
446
447
448
449
450
451
452
453
454
455
456
457
458
459
460

of the year circles are overlaid with triangles in ACCESS-S2, indicating that the ocean and atmosphere data assimilation is not affecting sea ice and that this component of the model is virtually free-running.

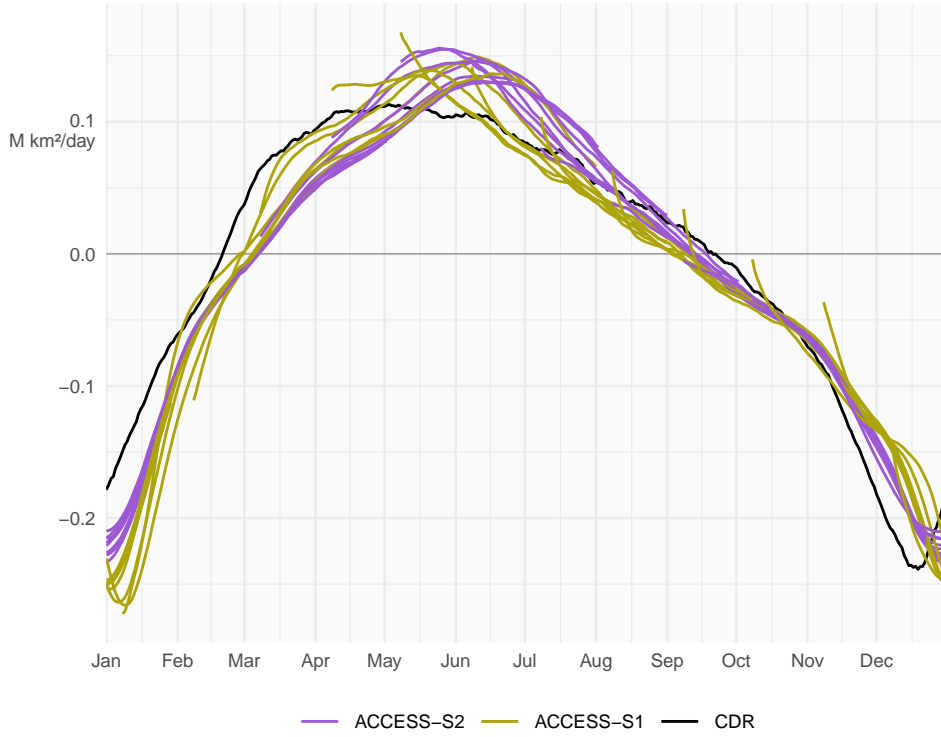
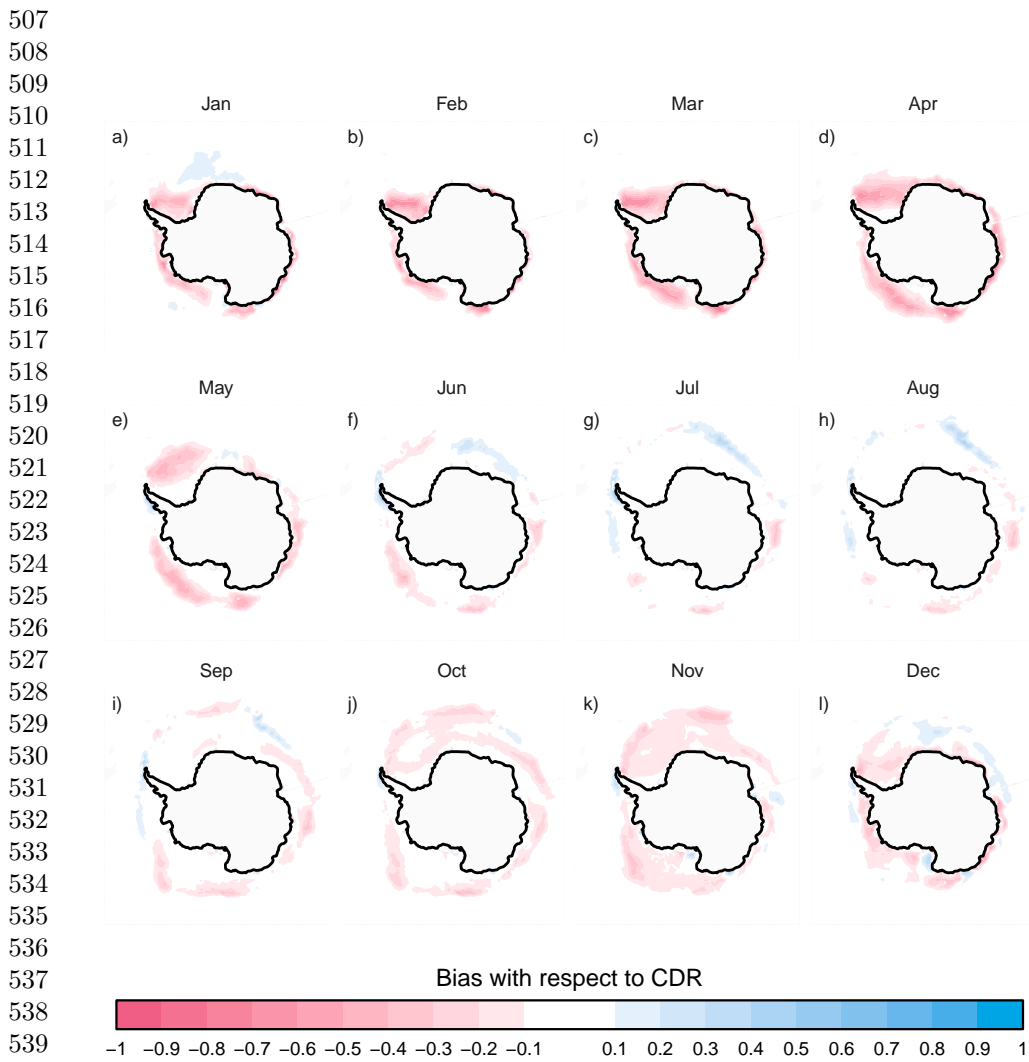


Figure 2: Mean daily sea-ice extent growth ($10^6 \text{ km}^2/\text{day}$) in ACCESS-S1 (green) and ACCESS-S2 (purple) hindcasts and observations (black), computed as the mean daily differences in sea-ice extent between each date and the next for each forecast month. Values are smoothed with a 11-day running mean.

To further understand the bias in ACCESS-S2, Figure 3 shows spatial patterns of the differences of monthly mean sea-ice concentrations between NOAA/NSIDC CDRV4 and ACCESS-S2 hindcasts at the shortest monthly lead time. From October to May, the model underestimates sea-ice concentrations in most regions except for the inner Weddell Sea in April and May, where sea-ice concentrations saturate to 1 both in the observations and forecasts. In winter, the differences are limited to a narrow



543 **Figure 3:** Ensemble mean difference between monthly sea-ice concentration of
 544 ACCESS-S2 ensemble mean forecast at 0-month lead time (monthly mean values fore-
 545 casted from the forecast initialised at the first of the month) and observations (CDR).

546
 547
 548 band around the sea-ice edge with slight positive biases in the African sector of
 549 East Antarctica and negative biases around the Indian Ocean sector which partially
 550 compensate, resulting in the near-zero extent bias seen in those months (Figure 1).
 551
 552

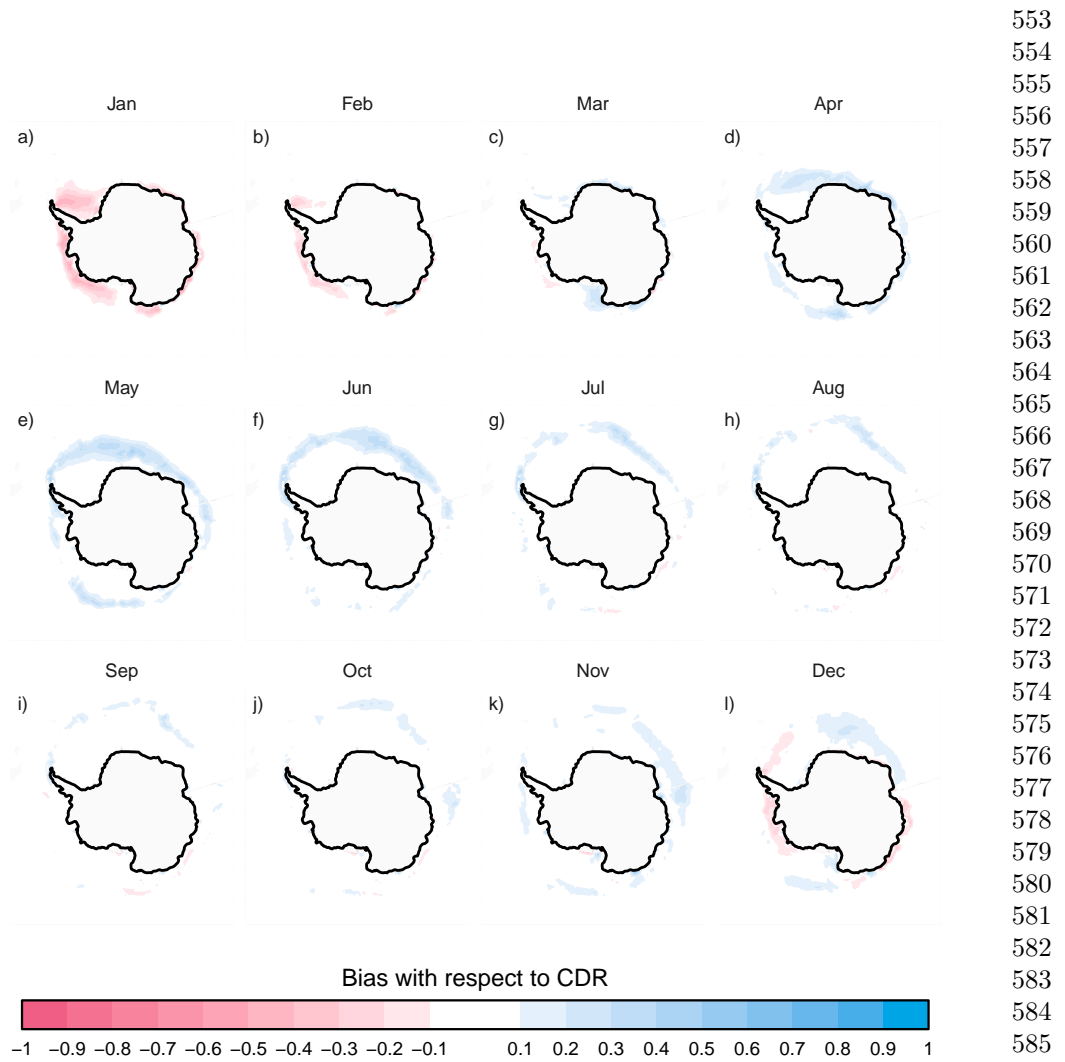


Figure 4: Same as Figure 3 but for ACCESS-S1.

ACCESS-S1 has a comparatively smaller overall bias (Figure 4). The largest values are found between April and June, when the faster growth results in large positive bias along the sea-ice edge, and in January, when the faster melt leads to large negative bias in the Weddell and Admunsen Seas.

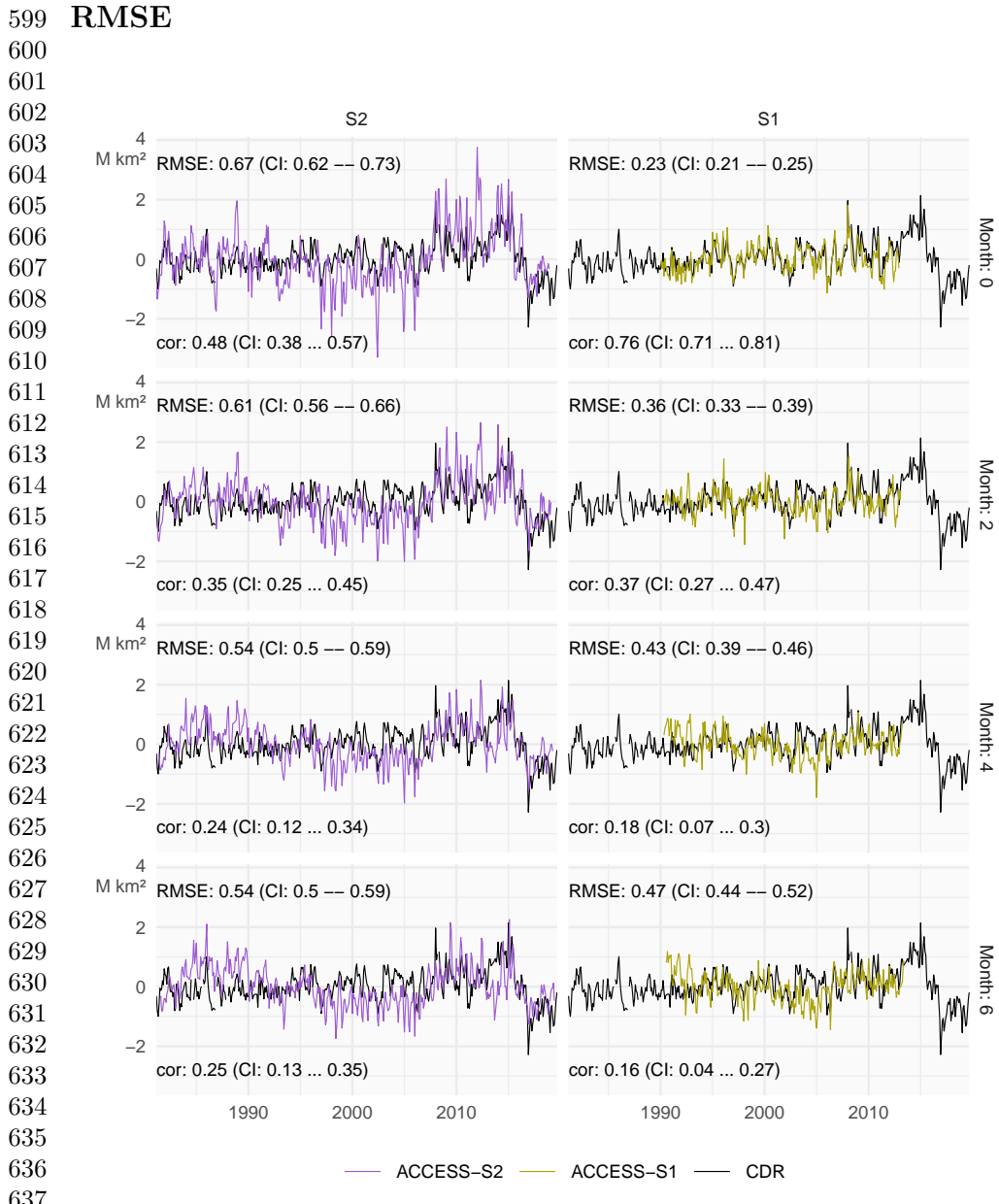


Figure 5 shows monthly sea-ice extent anomalies forecasted at selected lead times. 645
Compared with ACCESS-S1, ACCESS-S2 anomaly forecasts are relatively poor (large 646
RMSE) even for the first month (lead time 0), whereas ACCESS-S1 forecasts stay 647
relatively skilful even at a lead time of three months. ACCESS-S2 shows much larger 648
interannual variability than observations, with dramatic lows between 1995 and 2007, 649
and highs between 2007 and 2015. 650
651
652
653
654
655
656
657
658
659
660
661
662
663
664
665
666
667
668
669
670
671
672
673
674
675
676
677
678
679
680
681
682
683
684
685
686
687
688
689
690

Unexpectedly, for ACCESS-S2, RMSE improves with lead time, even though the correlation degrades with lead time. This is puzzling behaviour that goes contrary to what is usually seen in prediction models. The explanation seems to be the mentioned increased interannual variability. Figure 6 shows the interannual standard deviation of monthly sea-ice extent of the forecasts as a function of lead time compared with observations. ACCESS-S1 standard deviation lies within the observed standard deviation regardless of lead time, while ACCESS-S2 standard deviation is more than twice that of observations at zero lead time and only approaches the observed value at nine month lead time for most months.

ACCESS-S2 forecasts of sea-ice extent anomalies seem to align moderately well with observations (leading to moderately high correlation) but their magnitude is overestimated (leading to large errors). This could be caused by ACCESS-S2 sea ice being much more sensitive to atmospheric and oceanic forcing, perhaps due to lower thickness.

As an example, Figure 7 shows sea-ice concentration anomalies (top row) and sea-ice thickness and the difference between the two models (bottom row) for 2 May 2008 initialised one day prior; being that close to initialisation date, these are very approximately the initial conditions. ACCESS-S1 sea-ice concentrations anomalies are very close to observations as expected from the system assimilating these data. ACCESS-S2 sea-ice concentration anomalies, which are not assimilated, are not as close, but the large-scale pattern is aligned with observations. The system simulates large positive anomalies in the Weddell and Ross Seas and slight negative anomalies

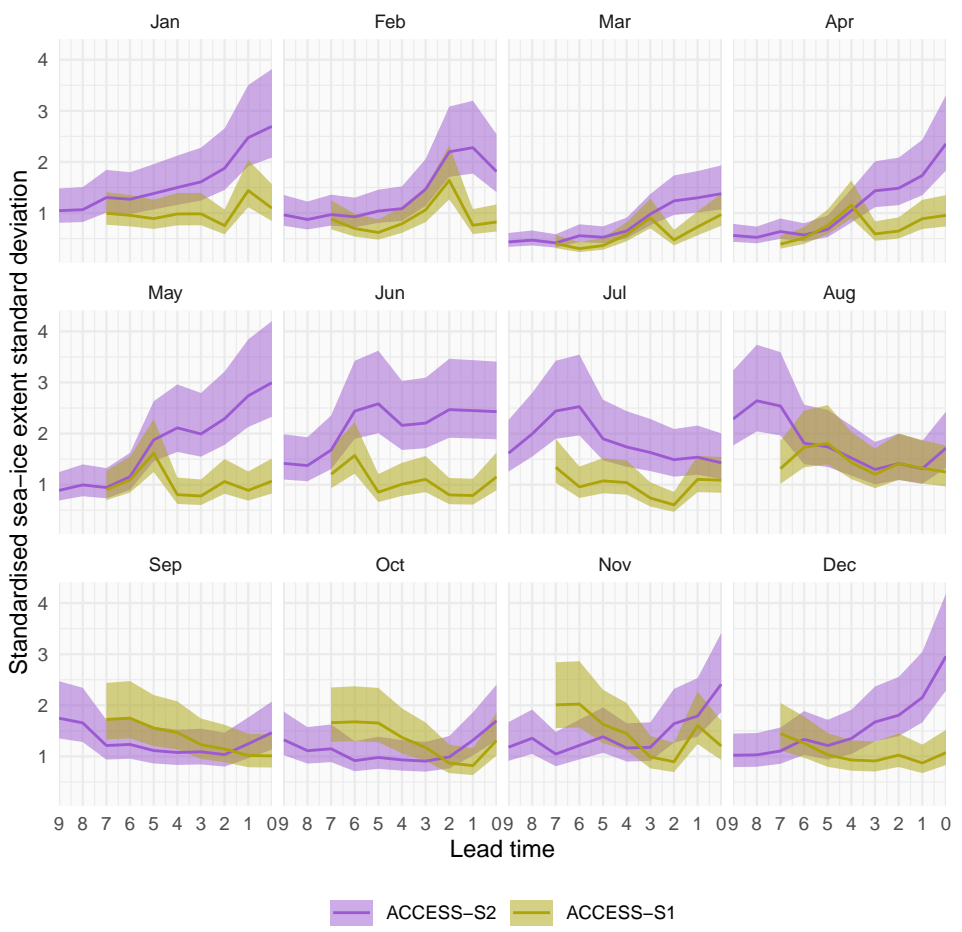


Figure 6: Interannual standard deviation with 95% confidence interval of monthly mean sea-ice extent forecasted for each month divided by that month's sea-ice extent observation standard deviation. ACCESS-S1 and ACCESS-S2 at different lead times. Each panel indicates the target month. Note the reverse horizontal axis.

in the Amundsen and Bellingshausen Seas. The fact that ACCESS-S2 can simulate this pattern without assimilating sea-ice data suggests that atmospheric and oceanic forcing were the dominant drivers. However, the magnitude of the sea-ice anomalies is too big. It is plausible that this is due to the thinner ice simulated by ACCESS-S2 (bottom row).

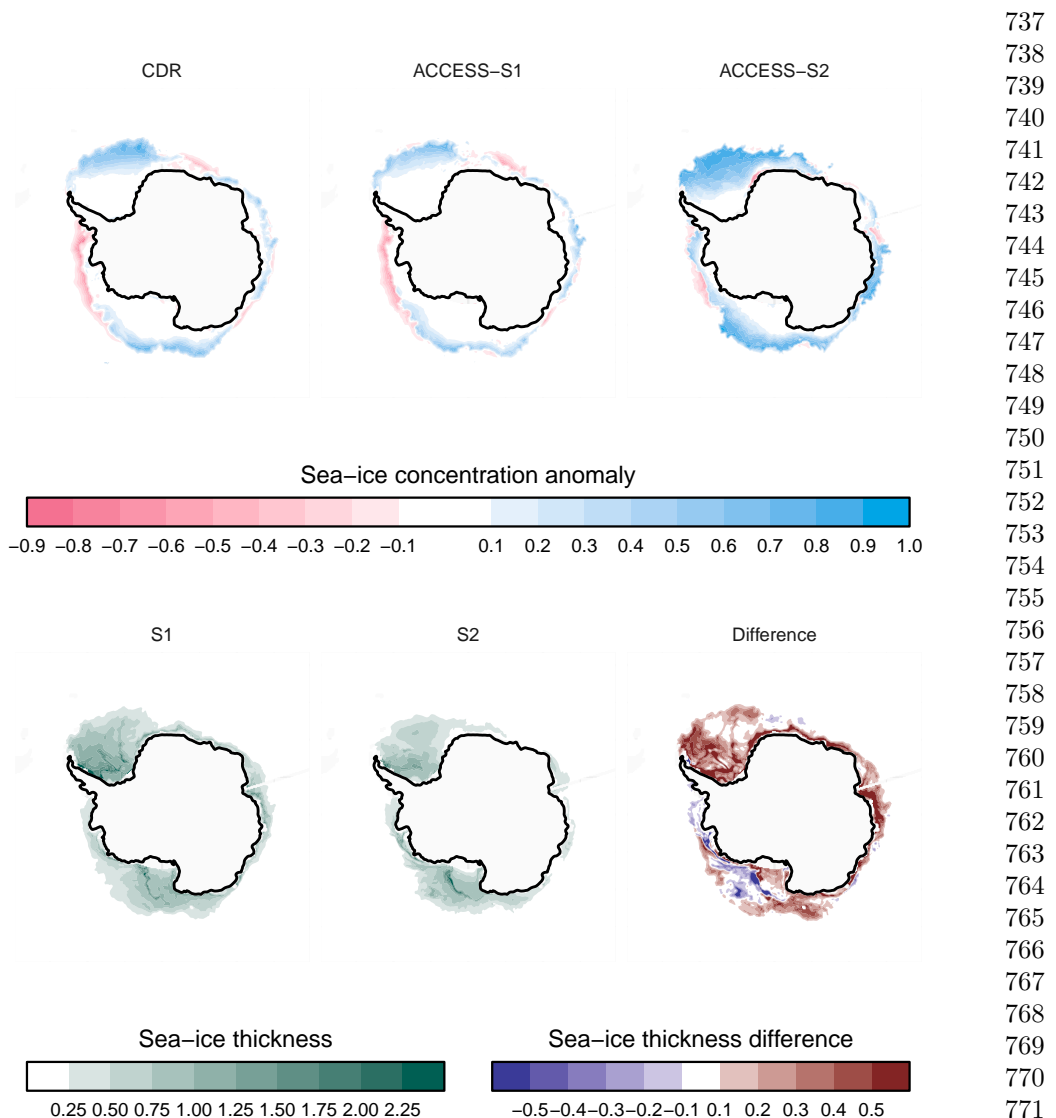
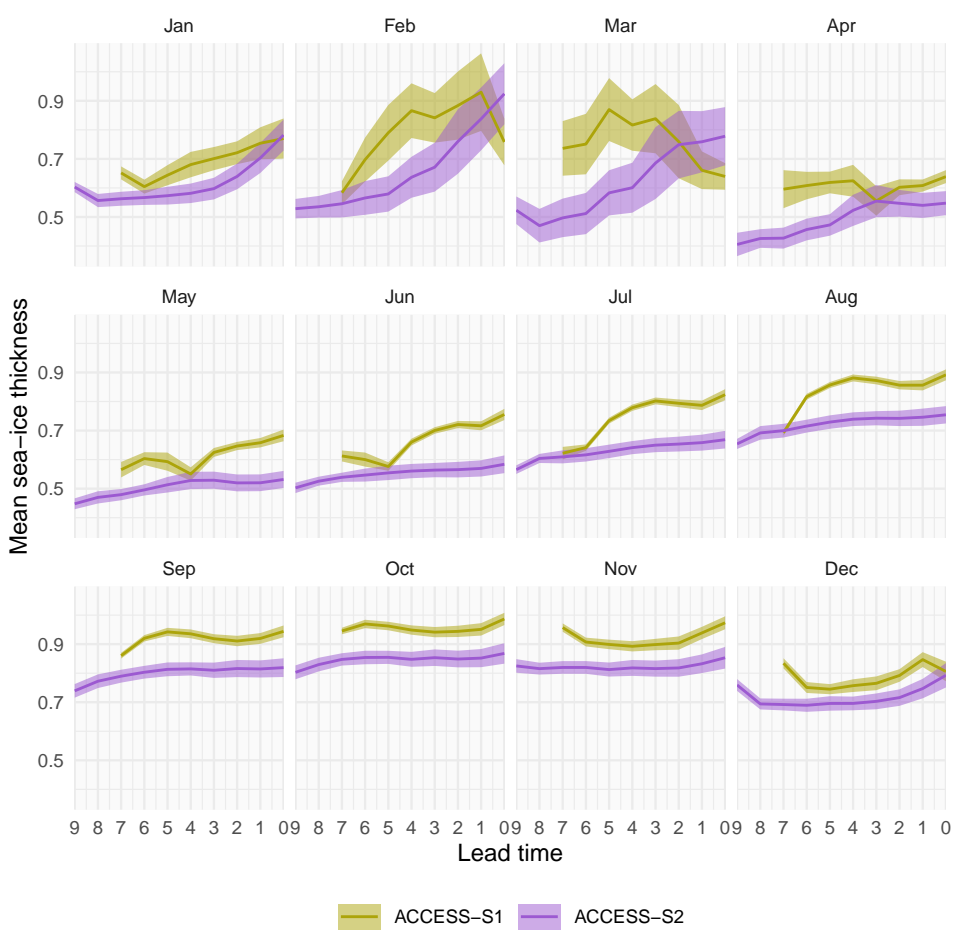


Figure 7: ACCESS-S1 and ACCESS-S2 hindcasts for 2 May 2008 at one day lead time. Top row shows sea-ice concentration anomalies forecasted by each system and the observations. Bottom row shows forecasted sea-ice thickness and the difference between ACCESS-S1 and ACCESS-S2.

Extending beyond the one case in Figure 7, Figure 8 shows monthly mean sea-ice thickness as a function of lead time for ACCESS-S1 and ACCESS-S2. Supporting the



813 **Figure 8:** Mean and 95% interval of monthly mean sea-ice thickness for ACCESS-S1
 814 and ACCESS-S2 at different lead times. Each panel indicates the target month. Note
 815 the reverse horizontal axis.

816
 817 idea that thinner ice is what causes the increased extent variability in ACCESS-S2,
 818 this system simulates thinner sea-ice compared to ACCESS-S1 overall at almost all
 819 lead times and in all months except for summer at short lead times (Dec-Jan, 0-1
 820 months; Feb-Mar, 0-2 months). However, in both systems, forecasted sea-ice is thicker
 821 at shorter lead times and then decreases, particularly in the summer months. If thinner
 822
 823
 824
 825
 826
 827
 828

ice were a sufficient cause of increased variability, then we would expect variability to
increase with lead time in both forecasting systems. 829
830
831
832
833
834
835
836
837
838
839
840
841
842
843
844
845
846
847
848
849
850
851
852
853
854
855
856
857
858
859
860
861
862
863
864
865
866
867
868
869
870
871
872
873
874

The fact that ACCESS-S1 and ACCESS-S2 share the same model configuration and
that the increased variability is more extreme at short lead times (Fig. 6) suggests
that the data assimilation procedure is partly responsible. It is possible that sea-ice in
the ACCESS-S2 system is left in an unbalanced state after assimilating atmospheric
and oceanic data but not sea-ice data, leading to large responses that are amplified
by the thin ice in the initial states which then subside at longer lead times when the
model is balanced.

To assess ACCESS-S2 forecasts in more detail, we compute error measures for all
hindcasts started on the 1st of every month.

Figure 9 shows the mean RMSE of sea-ice concentration anomalies for ACCESS-S1
and ACCESS-S2 hindcasts compared against persistence and climatological forecasts
used as a benchmark. Due to errors in the initial conditions, it is expected that
persistence forecasts would be better than the model forecasts at very short lead times,
but that the persistence forecast errors would grow faster and may eventually surpass
the model forecast errors. The black line shows that the persistence forecast error
indeed grows rapidly and reaches its maximum in about 30 days for most months
except for February, when it grows much slower. The ACCESS-S1 forecast errors grow
slower than persistence forecast errors and remain lower after less than 10 days on
average. The ACCESS-S2 forecast error starts high in all months and is lower than the
persistence forecast error after more than 15 days in most months except for forecast
initialised in February, when it takes 80 days.

At longer lead times, it is more appropriate to compare errors with the climatological
forecast error. The lead time at which ACCESS-S1 forecast error is higher than
the climatological forecast error varies between more than 60 and less than 20 days

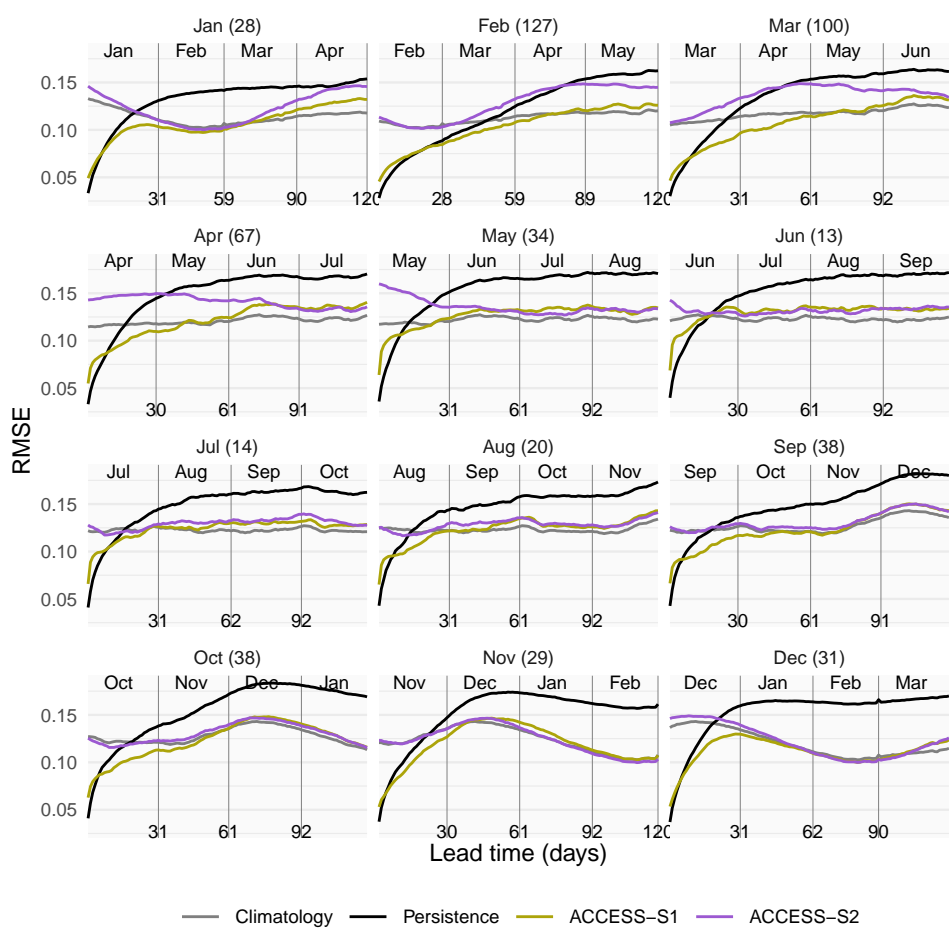


Figure 9: Mean RMSE of sea-ice concentration anomalies as a function of forecast lead time for all forecasts initialised on the first of each month compared with a reference forecast of persistence of anomalies (black) and climatology (gray). Only the first 120 days are shown. In parenthesis, the shortest time at which ACCESS-S1 and ACCESS-S2 mean RMSE is not statistically different at the 99% confidence level.

depending on forecast initialisation month with the minimum in June. ACCESS-S2 forecasts never have lower error than climatology, on the other hand, except marginally in October forecasts.

Figure 10 summarises the lead time window in which each hindcast is better than both the persistence forecast and the climatological forecast as a function of forecast

month. ACCESS-S1 forecasts have a wider lead time window in the summer than the other seasons and is not better than both benchmarks at forecasting June sea-ice concentration anomalies. Forecasts initialised in May and June are particularly poor, and July cannot be forecasted better than the benchmarks. This is consistent with the mid-winter loss of predictability observed by Libera et al. ⁴⁴, who attributed it to deep warm water entraining into the mixed layer.

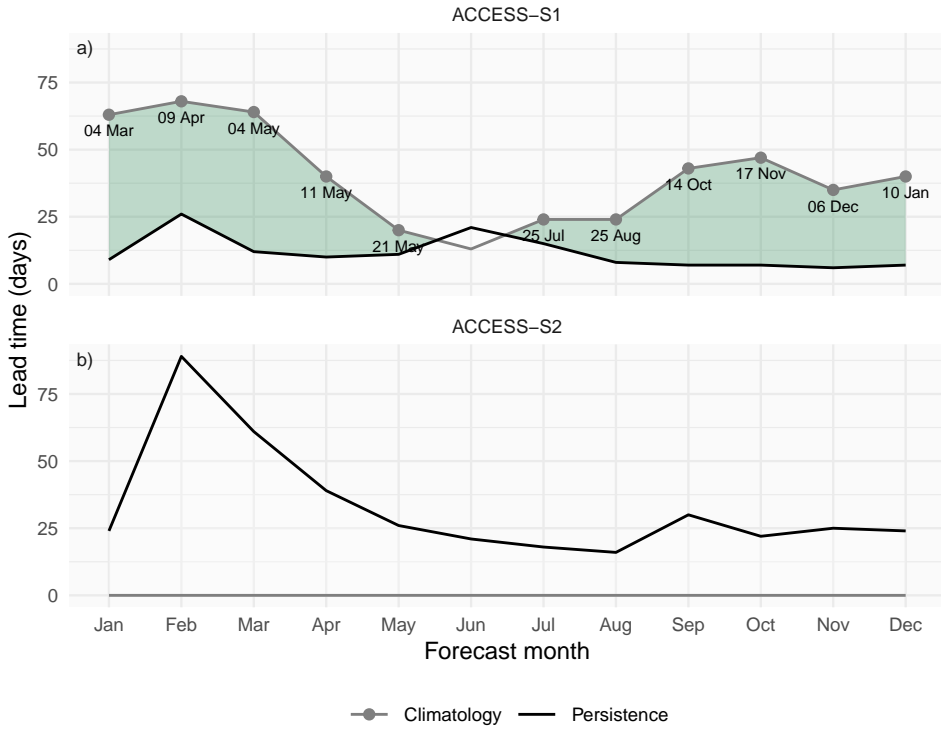


Figure 10: Minimum lead time at which each forecast's mean RMSE becomes larger than the lower bound of the 95% confidence interval of persistence forecast RMSE (black lines) and maximum lead time at which each forecast's mean RMSE remains lower than the lower bound of the 95% confidence interval of climatological forecast RMSE (gray lines). Green shading indicates the window where forecasts outperform both persistence (lead times longer than black line) and climatology (lead times shorter than gray line). Text labels show the date corresponding to the maximum lead time at which each forecast outperforms climatology.

921
922
923
924
925
926
927
928
929
930
931
932
933
934
935
936
937
938
939
940
941
942
943
944
945
946
947
948
949
950
951
952
953
954
955
956
957
958
959
960
961
962
963
964
965
966

967 To analyse the spatial distribution of the model error, we computed the RMSE of
968 zonal mean sea-ice concentration anomalies on 15 slices of 24° longitude span for each
969 forecasting system. We control for some areas being naturally easier to forecast than
970 others by computing the RMSE skill score with the climatological forecast RMSE as
971 reference.
972

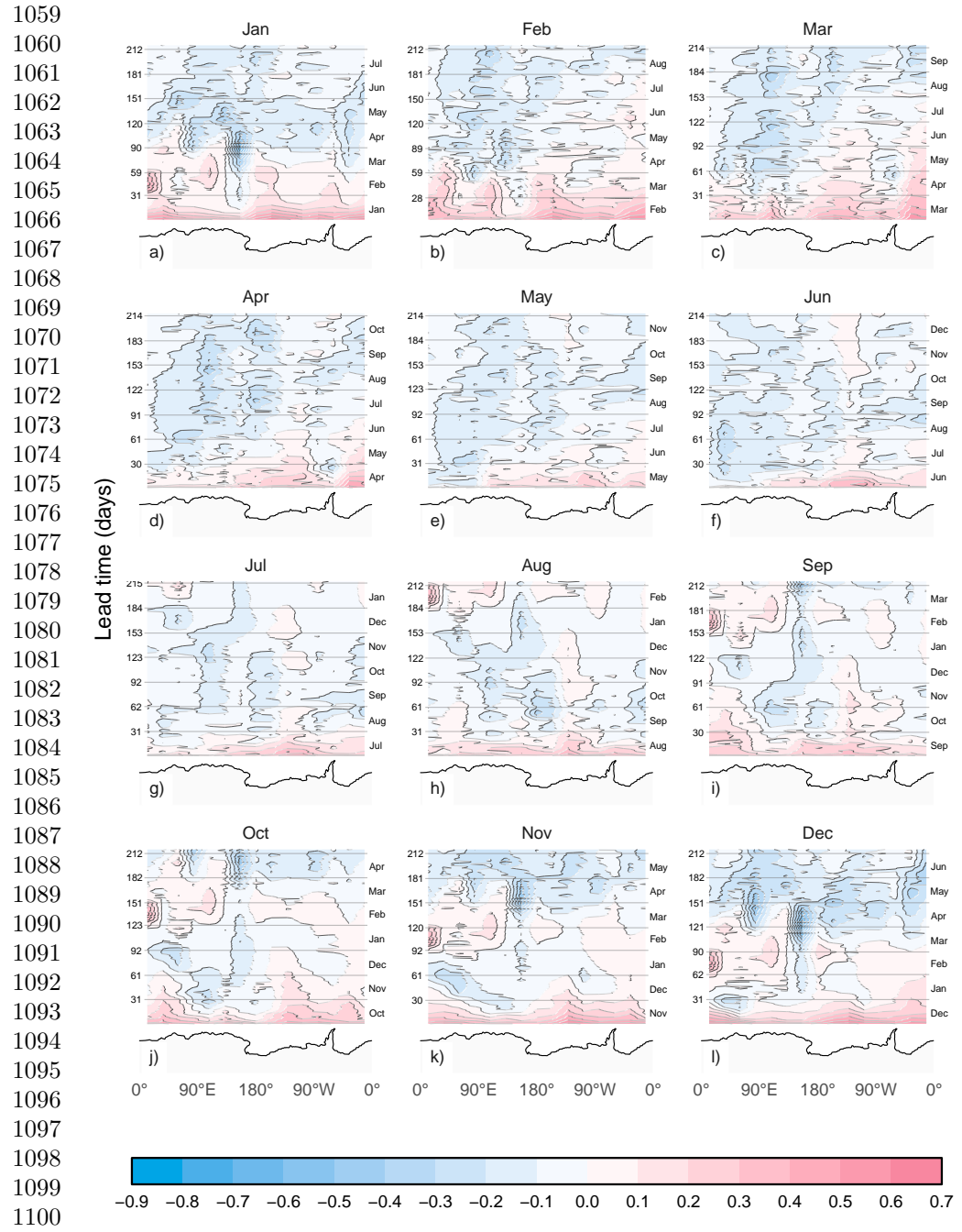
973
974 For ACCESS-S1 forecasts (Figure 11), skill tends to be lower off the coast of Eastern
975 Antarctica even at short lead times; for instance, the skill score for forecasts initialised
976 in May and June are negative between 0° and 120° E even at almost zero lead time.
977 This mirrors Libera et al.⁴⁴ findings of a “winter predictability barrier”, although they
978 focus on the Weddell Sea and here we show that the effect seems to be stronger more
979 to the east. In West Antarctica there is a hint of easterly-propagating skill in forecasts
980 initialised in February and March. This is consistent with Holland et al.¹³ findings
981 that memory of sea-ice anomalies are stored in ocean heat content anomalies that are
982 transported east by the Antarctic Circumpolar Current.
983

984
985 ACCESS-S2 forecasts (Figure 12) also have lower skill over East Antarctica. From
986 July to December even though the pan-Antarctic average skill is negative at all lead
987 times (Fig. 10), it is positive for up to a month in West Antarctica. Since oceanic and
988 atmospheric forcing is the only source of information, this suggests that sea-ice in
989 this region is particularly sensitive to oceanic and atmospheric forcing and suggests a
990 role of the Pacific-South American mode and the Amundsen Sea Low to shape sea-ice
991 concentration anomalies. The fact that this is evident in the months in which El Niño–
992 1000 concentration anomalies. The fact that this is evident in the months in which El Niño–
993 1001 Southern Oscillation teleconnections are more important for atmospheric circulation
994 1002 also suggest the influence of tropical Pacific variability. February and March are the
995 1003 only two months that can be forecasted with marginally positive skill in large regions.
996 1004
997 1005

998 1006 In Figure 9 the mean error was shown. Figure 13 column 1 shows the mean standard
999 1007 deviation of errors among ensemble members at various lead times. At one day lead
1000 1008 time (Fig. 13 a.1) ACCESS-S2 has a slightly larger spread than ACCESS-S1 due
1001 1009
1010 1011

to the way that ensemble members are generated. ACCESS-S1 ensemble members are generated by adding random field perturbations to the atmosphere only, which then are transferred to the other components via the coupled simulation¹⁷. With this scheme, ensemble members are all but guaranteed to be underdispersed in the ocean and sea-ice components. The time-lag ensemble used for ACCESS-S2 ensures greater spread. This difference is gone after about just two days, and both systems have a comparable spread in ensemble member error afterwards (Fig. 13 b1 and c1).

Figure 13 column 2, on the other hand, shows the standard deviation of ensemble mean error of each hindcast and the persistence forecast. At one day lead time, ACCESS-S2 ensemble mean error standard deviation is much larger than ACCESS-S1's, which in turn is comparable to the persistence forecast error standard deviation. At longer lead times, the spread of ACCESS-S1 and persistence forecast standard deviation increases to eventually be comparable to ACCESS-S2 and the standard deviation in climatological forecast errors. ACCESS-S2 error standard deviation is fairly independent of lead time and similar to the climatological forecast error standard deviation at all lead times.



1101 **Figure 11:** RMSE skill score of ACCESS-S1 forecasts with climatological forecast as
 1102 reference computed on 15 meridional slices 24° wide as a function of lead time and
 1103 longitude. Antarctica's coastline is shown at the bottom of each panel for reference.
 1104

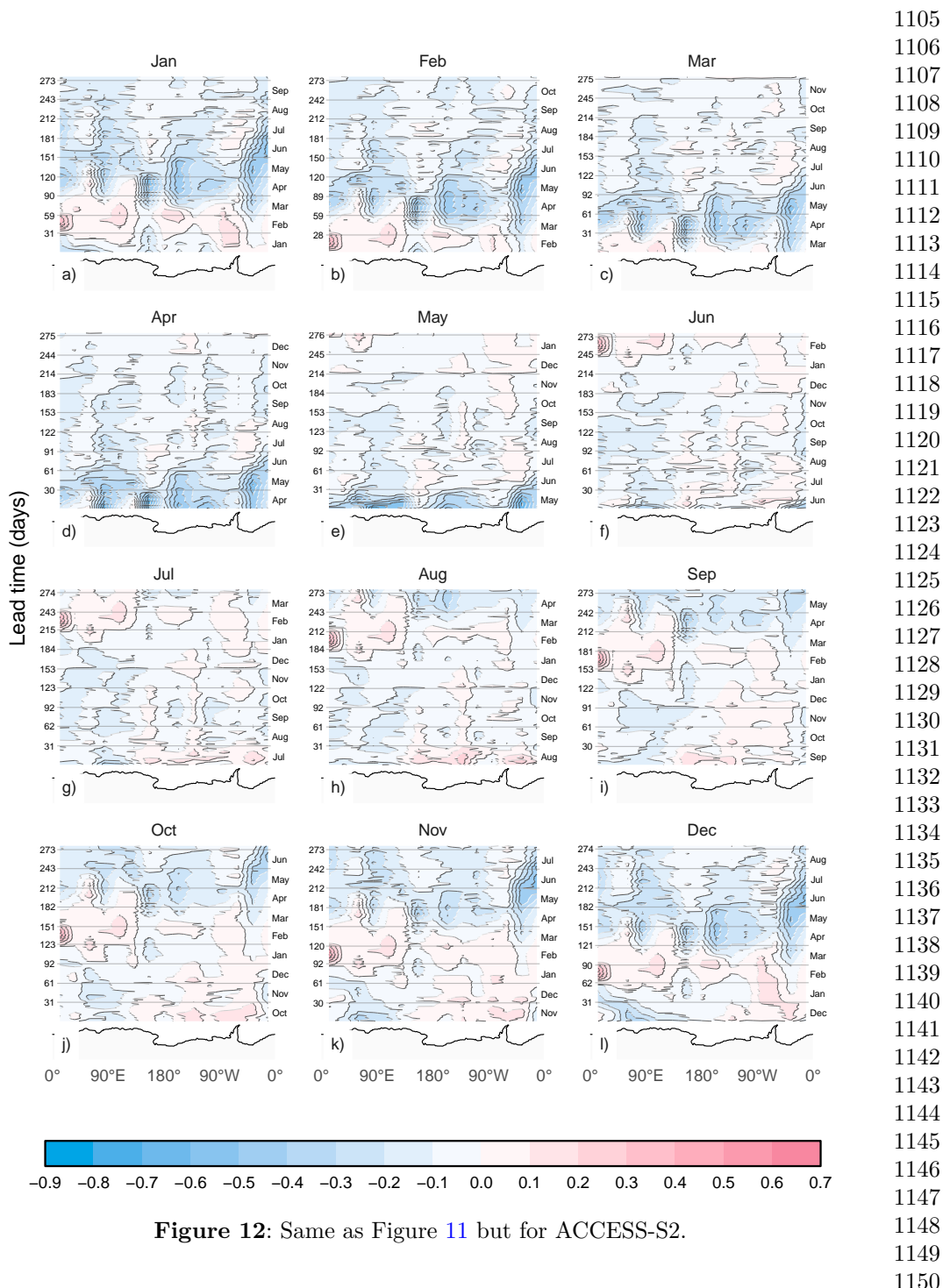
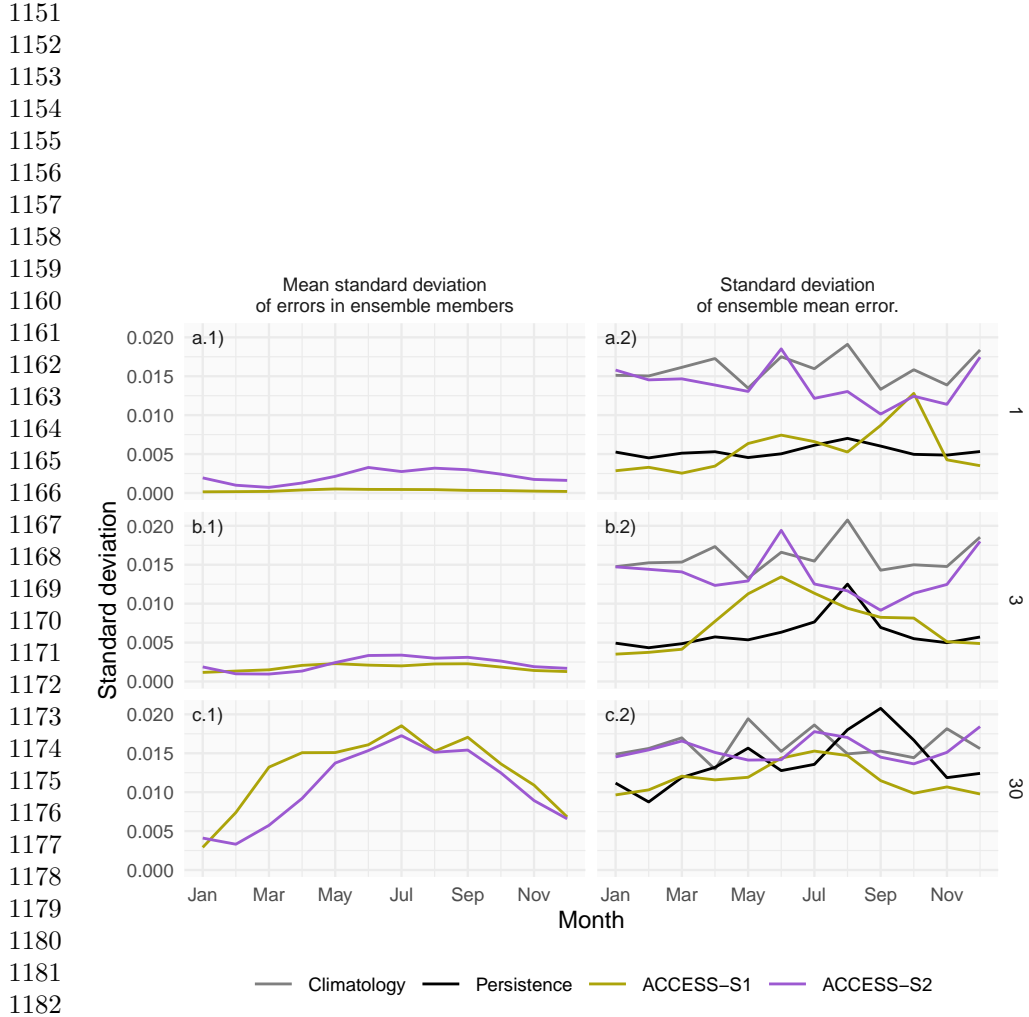


Figure 12: Same as Figure 11 but for ACCESS-S2.



1183 **Figure 13:** Decomposition of forecast error spread at 1, 5 and 30 days lead time for
 1184 ACCESS-S1 and ACCESS-S2 hindcasts across initialization months. The left column
 1185 shows the mean standard deviation of RMSE errors across ensemble members, while
 1186 the right column shows the standard deviation of the ensemble mean RMSE error and
 1187 the spread of the persistence and climatology forecasts errors.
 1188
 1189
 1190
 1191
 1192
 1193
 1194
 1195
 1196

Conclusions	1197
	1198
	1199
	1200
	1201
	1202
	1203
	1204
	1205
	1206
	1207
	1208
	1209
	1210
	1211
	1212
	1213
	1214
	1215
	1216
	1217
	1218
	1219
	1220
	1221
	1222
	1223
	1224
	1225
	1226
	1227
	1228
	1229
	1230
	1231
	1232
	1233
	1234
	1235
	1236
	1237
	1238
	1239
	1240
	1241
	1242
Sea-ice forecasts from the ACCESS-S2 system show a significant low extent bias, particularly during late summer and early autumn. This bias is attributed to a faster and longer melt season between January and March, and slower growth between March and April. This underestimation during the minimum and early freezing season is a common issue in many seasonal-to-subseasonal (S2S) systems, suggesting potential problems either with the model's thermodynamic representation or with short wave radiation forcing, as shown in other climate models ^{6;45} . Even though ACCESS-S2 shares the same model components as ACCESS-S1, the latter does not suffer from this bias, indicating that assimilating sea-ice concentrations successfully corrects for the negative bias that exists in the free-running model.	
Ensemble spread grows quickly even when perturbations are only implemented in the atmosphere component (in ACCESS-S1), indicating that sea ice is indeed responding quickly to atmospheric perturbations. However, our analysis suggests that the atmosphere and ocean data assimilation implemented in ACCESS-S2 is only effectively influencing sea-ice initial conditions from June to October, while the rest of the year, the sea-ice component runs virtually free, reverting to its biased equilibrium state.	
Analysis of the error spread shows that ACCESS-S2 initial conditions from December to May not only have large errors, but that the initial error spread is very large compared with ACCESS-S1. This spread is not due to the perturbation scheme, since the mean error variance for individual forecasts is low and comparable with ACCESS-S1. Instead, it is due to large variance of the mean error of individual forecasts, which is comparable to the climatology spread. This is further evidence that individual initial conditions are not being affected by the data assimilation scheme.	
Although ACCESS-S1 only assimilates sea-ice concentration, it is clear that sea-ice thickness is also affected through the assimilation process. ACCESS-S1 simulates	

1243 significantly thicker ice than ACCESS-S2 and in both systems sea-ice is thicker at
1244 shorter lead times than at longer lead times. Both the explicit data assimilation in
1245 ACCESS-S2 and the effects of atmospheric and oceanic data assimilation in ACCESS-
1246 S1 might be nudging simulated sea ice to be thicker than the model equilibrium
1247 state. We suggest that the thinner sea ice in ACCESS-S2 contributes to the large
1248 sea-ice extent variance, but other mechanisms, such as unbalanced initial conditions
1249 might also be important.
1250

1251 Given that ACCESS-S2 sea-ice extent is not directly initialised by sea-ice observations,
1252 comparing its forecasts with those of ACCESS-S1 allows us to estimate the time-
1253 scale over which initial conditions are important. We find that initial conditions affect
1254 Antarctic sea-ice forecasts in the order of a few months, but that effect is seasonally
1255 dependent. January to April initial conditions improve forecasts for up to three months
1256 with, February initial conditions in particular are shown to be crucial for determining
1257 sea-ice evolution at least up to May. Arctic sea-ice forecasts also show greater sensitivity
1258 to initial conditions in boreal summer, compared with boreal winter^{12;46}, suggesting a
1259 similar mechanism might be playing a role.
1260

1261 Forecasts initialised in winter have very little skill and ACCESS-S1 and ACCESS-S2
1262 forecast errors are not statistically different after just two weeks. This is consistent
1263 with the findings of Libera et al.⁴⁴'s finding of a "winter predictability barrier" in the
1264 Weddell Sea, although they describe the barrier as sharp loss of predictability in July,
1265 and here we find a gradual reduction in skill compared with climatology around June.
1266
1267 This difference might be due to our use of pan-Antarctic RMSE, since our regional
1268 analysis indicates that the degraded skill is most dramatic in the King Haakon sea.
1269
1270 These findings have important implications for both operational forecasting, model
1271 development and predictability studies. For operational centers, our results suggest that
1272 efforts to improve sea-ice data assimilation should prioritize the summer and autumn
1273 months when initial conditions have the greatest impact on forecast skill. Additionally,
1274

the substantial bias in ACCESS-S2 highlights the need for improved model physics,	1289
particularly in the representation of sea-ice thermodynamics and radiation processes.	1290
Crucially, our results suggest dramatic seasonal variations in sea-ice predictability.	1291
Future studies should therefore use initial conditions through the whole year rather	1292
than focusing on a limited number of initialisation dates.	1293
	1294
	1295
	1296
	1297
	1298
Acknowledgments	1299
	1300
	1301
This work was supported by ARC SRIEAS Grant SR200100005 Securing Antarctica's	1302
Environmental Future.	1303
	1304
	1305
	1306
	1307
Code and data availability	1308
	1309
The underlying code for this study is available on github and can be accessed via this	1310
link https://github.com/eliocamp/access-s2_ice-eval .	1311
Raw data of ACCESS-S1 and ACCESS-S2 forecast are not available due to size. Derived	1312
datasets required to reproduce the results are available in this zenodo repository:	1313
XXXXX	1314
	1315
	1316
	1317
	1318
	1319
	1320
References	1321
	1322
	1323
[1] De Silva, L.W.A., Inoue, J., Yamaguchi, H., Terui, T.: Medium range sea ice	1324
prediction in support of Japanese research vessel MIRAI's expedition cruise in	1325
2018. Polar Geography 43 (2-3), 223–239 (2020) https://doi.org/10.1080/1088937X.2019.1707317	1326
	1327
[2] Wagner, P.M., Hughes, N., Bourbonnais, P., Stroeve, J., Rabenstein, L., Bhatt,	1328
U., Little, J., Wiggins, H., Fleming, A.: Sea-ice information and forecast needs	1329
	1330
	1331
	1332
	1333
	1334

- 1335 for industry maritime stakeholders. *Polar Geography* **43**(2-3), 160–187 (2020)
1336
1337 <https://doi.org/10.1080/1088937X.2020.1766592>
- 1338
- 1339 [3] Rinke, A., Maslowski, W., Dethloff, K., Clement, J.: Influence of sea ice on the
1340 atmosphere: A study with an Arctic atmospheric regional climate model. *Journal*
1341 *of Geophysical Research: Atmospheres* **111**(D16) (2006) <https://doi.org/10.1029/2005JD006957>
- 1342
- 1343
- 1344 [4] Wang, Z., Fraser, A.D., Reid, P., Coleman, R., O'Farrell, S.: The Influence of
1345 Time-Varying Sea Ice Concentration on Antarctic and Southern Ocean Numerical
1346 Weather Prediction. *Weather and Forecasting* **39**(2), 293–310 (2024) <https://doi.org/10.1175/WAF-D-22-0220.1>. Chap. *Weather and Forecasting*
- 1347
- 1348
- 1349
- 1350
- 1351
- 1352
- 1353
- 1354 [5] Semmler, T., Kasper, M.A., Jung, T., Serrar, S.: Remote impact of the Antarctic
1355 atmosphere on the southern mid?latitudes. *Meteorologische Zeitschrift* **25**(1),
1356 71–77 (2016) <https://doi.org/10.1127/metz/2015/0685>
- 1357
- 1358
- 1359
- 1360 [6] Zampieri, L., Goessling, H.F., Jung, T.: Predictability of Antarctic Sea Ice Edge
1361 on Subseasonal Time Scales. *Geophysical Research Letters* **46**(16), 9719–9727
1362 (2019) <https://doi.org/10.1029/2019GL084096>
- 1363
- 1364
- 1365
- 1366 [7] Gao, Y., Xiu, Y., Nie, Y., Luo, H., Yang, Q., Zampieri, L., Lv, X., Uotila,
1367 P.: An Assessment of Subseasonal Prediction Skill of the Antarctic Sea Ice
1368 Edge. *Journal of Geophysical Research: Oceans* **129**(11), 2024–021499 (2024)
1369 <https://doi.org/10.1029/2024JC021499>
- 1370
- 1371
- 1372
- 1373 [8] Massonet, F., Barreira, S., Barthélémy, A., Bilbao, R., Blanchard-Wrigglesworth,
1374 E., Blockley, E., Bromwich, D.H., Bushuk, M., Dong, X., Goessling, H.F., Hobbs,
1375 W., Iovino, D., Lee, W.-S., Li, C., Meier, W.N., Merryfield, W.J., Moreno-
1376 Chamarro, E., Morioka, Y., Li, X., Niraula, B., Petty, A., Sanna, A., Scilingo, M.,
1377
- 1378
- 1379
- 1380

- Shu, Q., Sigmond, M., Sun, N., Tietsche, S., Wu, X., Yang, Q., Yuan, X.: SIPN South: Six years of coordinated seasonal Antarctic sea ice predictions. *Frontiers in Marine Science* **10** (2023) <https://doi.org/10.3389/fmars.2023.1148899> 1381
 1382
 1383
 1384
 1385
 1386
 1387
 1388
 1389
 1390
 1391
 1392
 1393
 1394
 1395
 1396
 1397
 1398
 1399
 1400
 1401
 1402
 1403
 1404
 1405
 1406
 1407
 1408
 1409
 1410
 1411
 1412
 1413
 1414
 1415
 1416
 1417
 1418
 1419
 1420
 1421
 1422
 1423
 1424
 1425
 1426
- [9] Dong, X., Yang, Q., Nie, Y., Zampieri, L., Wang, J., Liu, J., Chen, D.: Antarctic sea ice prediction with A convolutional long short-term memory network. *Ocean Modelling* **190**, 102386 (2024) <https://doi.org/10.1016/j.ocemod.2024.102386> 1381
 1382
 1383
 1384
 1385
 1386
 1387
 1388
 1389
 1390
 1391
 1392
 1393
 1394
 1395
 1396
 1397
 1398
 1399
 1400
 1401
 1402
 1403
 1404
 1405
 1406
 1407
 1408
 1409
 1410
 1411
 1412
 1413
 1414
 1415
 1416
 1417
 1418
 1419
 1420
 1421
 1422
 1423
 1424
 1425
 1426
- [10] Lin, Y., Yang, Q., Li, X., Dong, X., Luo, H., Nie, Y., Wang, J., Wang, Y., Min, C.: Ice-kNN-South: A Lightweight Machine Learning Model for Antarctic Sea Ice Prediction. *Journal of Geophysical Research: Machine Learning and Computation* **2**(1), 2024–000433 (2025) <https://doi.org/10.1029/2024JH000433> 1381
 1382
 1383
 1384
 1385
 1386
 1387
 1388
 1389
 1390
 1391
 1392
 1393
 1394
 1395
 1396
 1397
 1398
 1399
 1400
 1401
 1402
 1403
 1404
 1405
 1406
 1407
 1408
 1409
 1410
 1411
 1412
 1413
 1414
 1415
 1416
 1417
 1418
 1419
 1420
 1421
 1422
 1423
 1424
 1425
 1426
- [11] Guemas, V., Chevallier, M., Déqué, M., Bellprat, O., Doblas-Reyes, F.: Impact of sea ice initialization on sea ice and atmosphere prediction skill on seasonal timescales. *Geophysical Research Letters* **43**(8), 3889–3896 (2016) <https://doi.org/10.1002/2015GL066626> 1381
 1382
 1383
 1384
 1385
 1386
 1387
 1388
 1389
 1390
 1391
 1392
 1393
 1394
 1395
 1396
 1397
 1398
 1399
 1400
 1401
 1402
 1403
 1404
 1405
 1406
 1407
 1408
 1409
 1410
 1411
 1412
 1413
 1414
 1415
 1416
 1417
 1418
 1419
 1420
 1421
 1422
 1423
 1424
 1425
 1426
- [12] Day, J.J., Hawkins, E., Tietsche, S.: Will Arctic sea ice thickness initialization improve seasonal forecast skill? *Geophysical Research Letters* **41**(21), 7566–7575 (2014) <https://doi.org/10.1002/2014GL061694> 1381
 1382
 1383
 1384
 1385
 1386
 1387
 1388
 1389
 1390
 1391
 1392
 1393
 1394
 1395
 1396
 1397
 1398
 1399
 1400
 1401
 1402
 1403
 1404
 1405
 1406
 1407
 1408
 1409
 1410
 1411
 1412
 1413
 1414
 1415
 1416
 1417
 1418
 1419
 1420
 1421
 1422
 1423
 1424
 1425
 1426
- [13] Holland, M.M., Blanchard-Wrigglesworth, E., Kay, J., Vavrus, S.: Initial-value predictability of Antarctic sea ice in the Community Climate System Model 3. *Geophysical Research Letters* **40**(10), 2121–2124 (2013) <https://doi.org/10.1002/grl.50410> 1381
 1382
 1383
 1384
 1385
 1386
 1387
 1388
 1389
 1390
 1391
 1392
 1393
 1394
 1395
 1396
 1397
 1398
 1399
 1400
 1401
 1402
 1403
 1404
 1405
 1406
 1407
 1408
 1409
 1410
 1411
 1412
 1413
 1414
 1415
 1416
 1417
 1418
 1419
 1420
 1421
 1422
 1423
 1424
 1425
 1426
- [14] Marchi, S., Fichefet, T., Goosse, H.: Respective influences of perturbed atmospheric and ocean–sea ice initial conditions on the skill of seasonal Antarctic sea ice predictions: A study with NEMO3.6–LIM3. *Ocean Modelling* **148**, 101591 (2020) 1381
 1382
 1383
 1384
 1385
 1386
 1387
 1388
 1389
 1390
 1391
 1392
 1393
 1394
 1395
 1396
 1397
 1398
 1399
 1400
 1401
 1402
 1403
 1404
 1405
 1406
 1407
 1408
 1409
 1410
 1411
 1412
 1413
 1414
 1415
 1416
 1417
 1418
 1419
 1420
 1421
 1422
 1423
 1424
 1425
 1426

- 1427 <https://doi.org/10.1016/j.ocemod.2020.101591>
- 1428
- 1429 [15] Morioka, Y., Iovino, D., Cipollone, A., Masina, S., Behera, S.K.: Decadal Sea
- 1430 Ice Prediction in the West Antarctic Seas with Ocean and Sea Ice Initializations.
- 1431
- 1432 Communications Earth & Environment **3**(1), 189 (2022) <https://doi.org/10.1038/s43247-022-00529-z>
- 1433
- 1434
- 1435
- 1436
- 1437 [16] Wedd, R., Alves, O., Burgh-Day, C., Down, C., Griffiths, M., Hendon, H.H.,
- 1438 Hudson, D., Li, S., Lim, E.-P., Marshall, A.G., Shi, L., Smith, P., Smith, G.,
- 1439 Spillman, C.M., Wang, G., Wheeler, M.C., Yan, H., Yin, Y., Young, G., Zhao, M.,
- 1440 Xiao, Y., Zhou, X.: ACCESS-S2: The upgraded Bureau of Meteorology multi-week
- 1441 to seasonal prediction system. Journal of Southern Hemisphere Earth Systems
- 1442
- 1443 Science **72**(3), 218–242 (2022) <https://doi.org/10.1071/ES22026>
- 1444
- 1445
- 1446
- 1447
- 1448 [17] Hudson, D., Alves, O., Hendon, H.H., Lim, E.-P., Liu, G., Luo, J.-J., MacLachlan,
- 1449 C., Marshall, A.G., Shi, L., Wang, G., Wedd, R., Young, G., Zhao, M., Zhou, X.:
- 1450 ACCESS-S1 The new Bureau of Meteorology multi-week to seasonal prediction
- 1451 system. Journal of Southern Hemisphere Earth Systems Science **67**(3), 132–159
- 1452
- 1453
- 1454 (2017) <https://doi.org/10.1071/es17009>
- 1455
- 1456
- 1457 [18] Williams, K.D., Harris, C.M., Bodas-Salcedo, A., Camp, J., Comer, R.E., Copsey,
- 1458 D., Fereday, D., Graham, T., Hill, R., Hinton, T., Hyder, P., Ineson, S., Masato,
- 1459 G., Milton, S.F., Roberts, M.J., Rowell, D.P., Sanchez, C., Shelly, A., Sinha, B.,
- 1460 Walters, D.N., West, A., Woollings, T., Xavier, P.K.: The Met Office Global
- 1461 Coupled model 2.0 (GC2) configuration. Geoscientific Model Development **8**(5),
- 1462 1509–1524 (2015) <https://doi.org/10.5194/gmd-8-1509-2015>
- 1463
- 1464
- 1465
- 1466
- 1467
- 1468 [19] Waters, J., Bell, M.J., Martin, M.J., Lea, D.J.: Reducing ocean model imbalances
- 1469 in the equatorial region caused by data assimilation. Quarterly Journal of the Royal
- 1470 Meteorological Society **143**(702), 195–208 (2017) <https://doi.org/10.1002/qj.2912>
- 1471
- 1472

- [20] Best, M.J., Pryor, M., Clark, D.B., Rooney, G.G., Essery, R.L.H., Ménard, C.B., Edwards, J.M., Hendry, M.A., Porson, A., Gedney, N., Mercado, L.M., Sitch, S., Blyth, E., Boucher, O., Cox, P.M., Grimmond, C.S.B., Harding, R.J.: The Joint UK Land Environment Simulator (JULES), model description – Part 1: Energy and water fluxes. *Geoscientific Model Development* **4**(3), 677–699 (2011) <https://doi.org/10.5194/gmd-4-677-2011> 1473
1474
1475
1476
1477
1478
1479
1480
1481
1482
1483
1484
1485
1486
1487
1488
1489
1490
1491
1492
1493
1494
1495
1496
1497
1498
1499
1500
1501
1502
1503
1504
1505
1506
1507
1508
1509
1510
1511
1512
1513
1514
1515
1516
1517
1518
- [21] Gurvan, M., Bourdallé-Badie, R., Bouttier, P.-A., Bricaud, C., Bruciaferri, D., Calvert, D., Chanut, J., Clementi, E., Coward, A., Delrosso, D., Ethé, C., Flavoni, S., Graham, T., Harle, J., Iovino, D., Lea, D., Lévy, C., Lovato, T., Martin, N., Masson, S., Mocavero, S., Paul, J., Rousset, C., Storkey, D., Storto, A., Vancoppenolle, M.: NEMO ocean engine (2013) <https://doi.org/10.5281/zenodo.1475234> 1483
1484
1485
1486
1487
1488
1489
1490
1491
1492
1493
1494
1495
1496
1497
1498
1499
1500
1501
1502
1503
1504
1505
1506
1507
1508
1509
1510
1511
1512
1513
1514
1515
1516
1517
1518
- [22] Megann, A., Storkey, D., Aksenov, Y., Alderson, S., Calvert, D., Graham, T., Hyder, P., Siddorn, J., Sinha, B.: GO5.0: The joint NERC–Met Office NEMO global ocean model for use in coupled and forced applications. *Geoscientific Model Development* **7**(3), 1069–1092 (2014) <https://doi.org/10.5194/gmd-7-1069-2014> 1494
1495
1496
1497
1498
1499
1500
1501
1502
1503
1504
1505
1506
1507
1508
1509
1510
1511
1512
1513
1514
1515
1516
1517
1518
- [23] Rae, J.G.L., Hewitt, H.T., Keen, A.B., Ridley, J.K., West, A.E., Harris, C.M., Hunke, E.C., Walters, D.N.: Development of the Global Sea Ice 6.0 CICE configuration for the Met Office Global Coupled model. *Geoscientific Model Development* **8**(7), 2221–2230 (2015) <https://doi.org/10.5194/gmd-8-2221-2015> 1509
1510
1511
1512
1513
1514
1515
1516
1517
1518
- [24] Dee, D.P., Uppala, S.M., Simmons, A.J., Berrisford, P., Poli, P., Kobayashi, S., Andrae, U., Balmaseda, M.A., Balsamo, G., Bauer, P., Bechtold, P., Beljaars, A.C.M., van de Berg, L., Bidlot, J., Bormann, N., Delsol, C., Dragani, R., Fuentes, M., Geer, A.J., Haimberger, L., Healy, S.B., Hersbach, H., Hólm, E.V., Isaksen, L., Kållberg, P., Köhler, M., Matricardi, M., McNally, A.P., Monge-Sanz, B.M., 33

- 1519 Morcrette, J.-J., Park, B.-K., Peubey, C., de Rosnay, P., Tavolato, C., Thépaut,
1520 J.-N., Vitart, F.: The ERA-Interim reanalysis: Configuration and performance
1521 of the data assimilation system. *Quarterly Journal of the Royal Meteorological*
1522 Society **137**(656), 553–597 (2011) <https://doi.org/10.1002/qj.828>
- 1523
1524
1525
1526 [25] Waters, J., Lea, D.J., Martin, M.J., Mirouze, I., Weaver, A., While, J.: Imple-
1527 menting a variational data assimilation system in an operational 1/4 degree global
1528 ocean model. *Quarterly Journal of the Royal Meteorological Society* **141**(687),
1529 333–349 (2015) <https://doi.org/10.1002/qj.2388>
- 1530
1531
1532
1533 [26] Good, S.A., Martin, M.J., Rayner, N.A.: EN4: Quality controlled ocean tem-
1534 perature and salinity profiles and monthly objective analyses with uncertainty
1535 estimates. *Journal of Geophysical Research: Oceans* **118**(12), 6704–6716 (2013)
1536
1537 <https://doi.org/10.1002/2013JC009067>
- 1538
1539
1540
1541 [27] Reynolds, R.W., Smith, T.M., Liu, C., Chelton, D.B., Casey, K.S., Schlax, M.G.:
1542 Daily High-Resolution-Blended Analyses for Sea Surface Temperature. *Journal*
1543 of Climate **20**(22), 5473–5496 (2007) <https://doi.org/10.1175/2007JCLI1824.1> .
1544
1545
1546 Chap. *Journal of Climate*
1547
1548
1549 [28] Zweng, M.M., Reagan, J.R., Antonov, J.I., Locarnini, R.A., Mishonov, A.V.,
1550 Boyer, T.P., Garcia, H.E., Baranova, O.K., Johnson, D.R., Seidov, D., Biddle,
1551 M.M.: World ocean atlas 2013. Volume 2, Salinity (2013) <https://doi.org/10.7289/V5251G4D>
1552
1553
1554
1555
1556 [29] Meier, W.N., Stewart, J.S.: Assessing uncertainties in sea ice extent climate
1557 indicators. *Environmental Research Letters* **14**(3), 035005 (2019) <https://doi.org/10.1088/1748-9326/aaf52c>
- 1558
1559
1560
1561
1562
1563
1564

- [30] Meier, W.N., Peng, G., Scott, D.J., Savoie, M.H.: Verification of a new NOAA/N-SIDC passive microwave sea-ice concentration climate record. *Polar Research* (2014) <https://doi.org/10.3402/polar.v33.21004> 1565
1566
1567
1568
1569
1570
1571
1572
1573
1574
1575
1576
1577
1578
1579
1580
1581
1582
1583
1584
1585
1586
1587
1588
1589
1590
1591
1592
1593
1594
1595
1596
1597
1598
1599
1600
1601
1602
1603
1604
1605
1606
1607
1608
1609
1610
- [31] Cavalieri, D.J., Gloersen, P., Campbell, W.J.: Determination of sea ice parameters with the NIMBUS 7 SMMR. *Journal of Geophysical Research: Atmospheres* **89**(D4), 5355–5369 (1984) <https://doi.org/10.1029/JD089iD04p05355> 1565
1566
1567
1568
1569
1570
1571
1572
1573
1574
1575
1576
1577
1578
1579
1580
1581
1582
1583
1584
1585
1586
1587
1588
1589
1590
1591
1592
1593
1594
1595
1596
1597
1598
1599
1600
1601
1602
1603
1604
1605
1606
1607
1608
1609
1610
- [32] Comiso, J.: Bootstrap Sea Ice Concentrations from Nimbus-7 SMMR and DMSP SSM/I-SSMIS. (NSIDC-0079, Version 4). NASA National Snow and Ice Data Center Distributed Active Archive Center., Boulder, Colorado USA. (2023). <https://doi.org/10.5067/X5LG68MH013O> 1565
1566
1567
1568
1569
1570
1571
1572
1573
1574
1575
1576
1577
1578
1579
1580
1581
1582
1583
1584
1585
1586
1587
1588
1589
1590
1591
1592
1593
1594
1595
1596
1597
1598
1599
1600
1601
1602
1603
1604
1605
1606
1607
1608
1609
1610
- [33] Meier, W.N., Fetterer, F., Windnagel, A.K., Stewart, J.S.: NOAA/NSIDC Climate Data Record of Passive Microwave Sea Ice Concentration. National Snow and Ice Data Center., Boulder, Colorado USA (2021). <https://doi.org/10.7265/efmz-2t65> 1565
1566
1567
1568
1569
1570
1571
1572
1573
1574
1575
1576
1577
1578
1579
1580
1581
1582
1583
1584
1585
1586
1587
1588
1589
1590
1591
1592
1593
1594
1595
1596
1597
1598
1599
1600
1601
1602
1603
1604
1605
1606
1607
1608
1609
1610
- [34] EUMETSAT Ocean and Sea Ice Satellite Application Facility: Global Sea Ice Concentration Climate Data Record 1978-2020 (v3.0, 2022), OSI-450-a, <https://cds.climate.copernicus.eu/cdsapp#!/dataset/satellite-sea-ice-concentration> 1565
1566
1567
1568
1569
1570
1571
1572
1573
1574
1575
1576
1577
1578
1579
1580
1581
1582
1583
1584
1585
1586
1587
1588
1589
1590
1591
1592
1593
1594
1595
1596
1597
1598
1599
1600
1601
1602
1603
1604
1605
1606
1607
1608
1609
1610
- [35] Cavalieri, D.J., Crawford, J.P., Drinkwater, M.R., Eppler, D.T., Farmer, L.D., Jentz, R.R., Wackerman, C.C.: Aircraft active and passive microwave validation of sea ice concentration from the Defense Meteorological Satellite Program special sensor microwave imager. *Journal of Geophysical Research: Oceans* **96**(C12), 21989–22008 (1991) <https://doi.org/10.1029/91JC02335> 1565
1566
1567
1568
1569
1570
1571
1572
1573
1574
1575
1576
1577
1578
1579
1580
1581
1582
1583
1584
1585
1586
1587
1588
1589
1590
1591
1592
1593
1594
1595
1596
1597
1598
1599
1600
1601
1602
1603
1604
1605
1606
1607
1608
1609
1610
- [36] Murphy, A.H., Daan, H.: Forecast Evaluation. In: *Probability, Statistics, And Decision Making In The Atmospheric Sciences*. CRC Press, ??? (1985) 1565
1566
1567
1568
1569
1570
1571
1572
1573
1574
1575
1576
1577
1578
1579
1580
1581
1582
1583
1584
1585
1586
1587
1588
1589
1590
1591
1592
1593
1594
1595
1596
1597
1598
1599
1600
1601
1602
1603
1604
1605
1606
1607
1608
1609
1610
- [37] R Core Team: R: A Language and Environment for Statistical Computing. R 1565
1566
1567
1568
1569
1570
1571
1572
1573
1574
1575
1576
1577
1578
1579
1580
1581
1582
1583
1584
1585
1586
1587
1588
1589
1590
1591
1592
1593
1594
1595
1596
1597
1598
1599
1600
1601
1602
1603
1604
1605
1606
1607
1608
1609
1610

1611 Foundation for Statistical Computing, Vienna, Austria (2020). R Foundation for
1612 Statistical Computing
1613
1614
1615 [38] Dowle, M., Srinivasan, A.: Data.Table: Extension of 'Data.Frame' (2020)
1616
1617
1618 [39] Campitelli, E.: metR: Tools for Easier Analysis of Meteorological Fields (2020)
1619
1620 [40] Schulzweida, U.: CDO User Guide (2023) <https://doi.org/10.5281/ZENODO.10020800>
1621
1622
1623
1624 [41] Wickham, H.: Ggplot2: Elegant Graphics for Data Analysis. Use R! Springer,
1625
1626 New York (2009). <https://doi.org/10.1007/978-0-387-98141-3>
1627
1628 [42] Xie, Y.: Dynamic Documents with R and Knitr, 2nd edn. Chapman and Hall/CRC,
1629
1630 Boca Raton, Florida (2015)
1631
1632
1633 [43] Allaire, J.J., Teague, C., Xie, Y., Dervieux, C.: Quarto. Zenodo (2022). <https://doi.org/10.5281/ZENODO.5960048>
1634
1635
1636
1637 [44] Libera, S., Hobbs, W., Klocker, A., Meyer, A., Matear, R.: Ocean-Sea Ice
1638 Processes and Their Role in Multi-Month Predictability of Antarctic Sea Ice.
1639
1640 Geophysical Research Letters **49**(8), 2021–097047 (2022) <https://doi.org/10.1029/2021GL097047>
1641
1642
1643
1644 [45] Roach, L.A., Dörr, J., Holmes, C.R., Massonnet, F., Blockley, E.W., Notz, D.,
1645
1646 Rackow, T., Raphael, M.N., O'Farrell, S.P., Bailey, D.A., Bitz, C.M.: Antarctic
1647
1648 Sea Ice Area in CMIP6. Geophysical Research Letters **47**(9), 2019–086729 (2020)
1649 <https://doi.org/10.1029/2019GL086729>
1650
1651
1652 [46] Bunzel, F., Notz, D., Baehr, J., Müller, W.A., Fröhlich, K.: Seasonal climate
1653 forecasts significantly affected by observational uncertainty of Arctic sea ice
1654 concentration. Geophysical Research Letters **43**(2), 852–859 (2016) <https://doi.org/10.1029/2015GL065614>
1655
1656

org/10.1002/2015GL066928	1657
	1658
	1659
	1660
	1661
	1662
	1663
	1664
	1665
	1666
	1667
	1668
	1669
	1670
	1671
	1672
	1673
	1674
	1675
	1676
	1677
	1678
	1679
	1680
	1681
	1682
	1683
	1684
	1685
	1686
	1687
	1688
	1689
	1690
	1691
	1692
	1693
	1694
	1695
	1696
	1697
	1698
	1699
	1700
	1701
	1702

1703 **Supplementary figures**

1704

1705

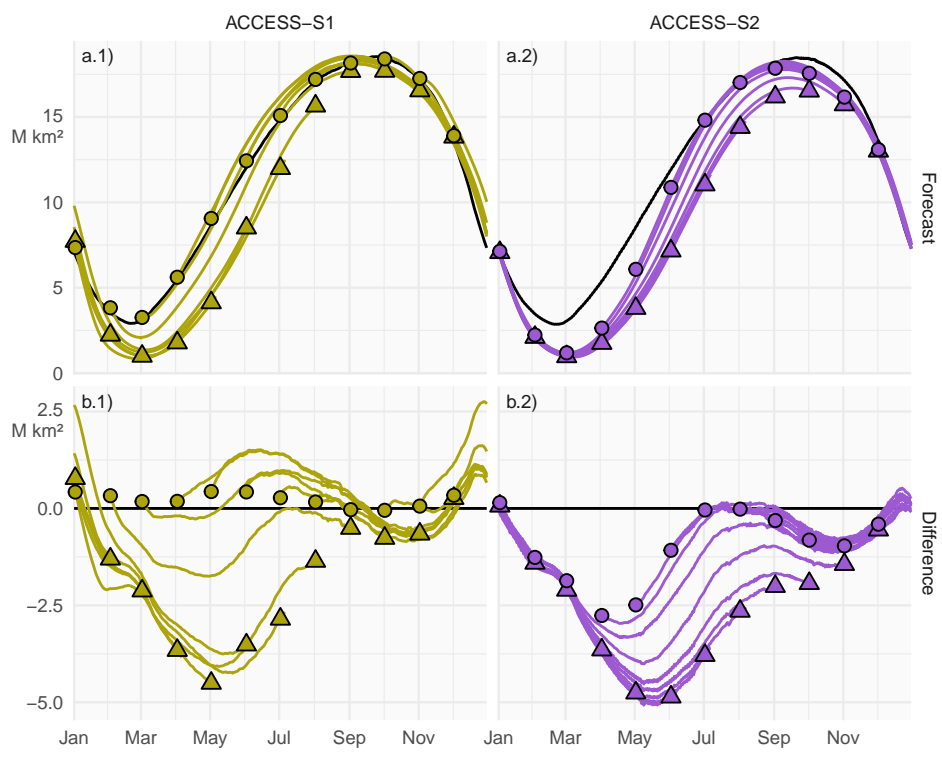
1706 The following are the same figures from the main paper but using the OSI dataset
 1707 instead of CDR.

1708

1709

1710

1711



1734 **Figure A1:** Row a: Pan-Antarctic mean sea-ice extent for all hindcasts initialised on
 1735 the first of each calendar month for ACCESS-S1 (column 1; green) and ACCESS-S1
 1736 (column 2; purple). Observed mean sea-ice extent in each corresponding hindcast period
 1737 is shown in black. Row b: Mean differences between the forecast and the observed
 1738 values. Circles represent the initial conditions at the start of forecasts (i.e., the first of
 1739 every month), and triangles represent the mean values at the end of forecasts (i.e., the
 1740 longest possible lead time).

1741

1742

1743

1744

1745

1746

1747

1748

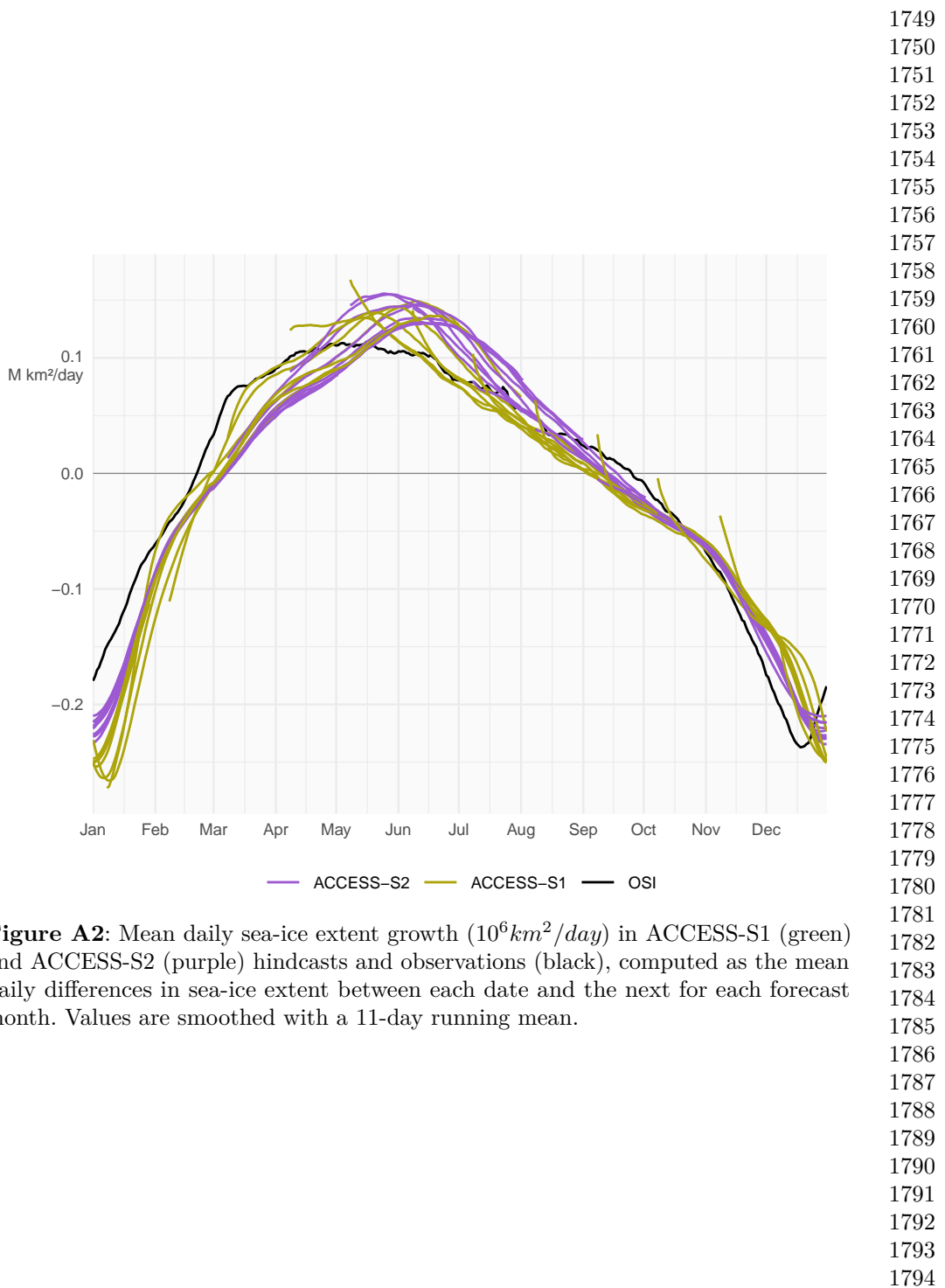
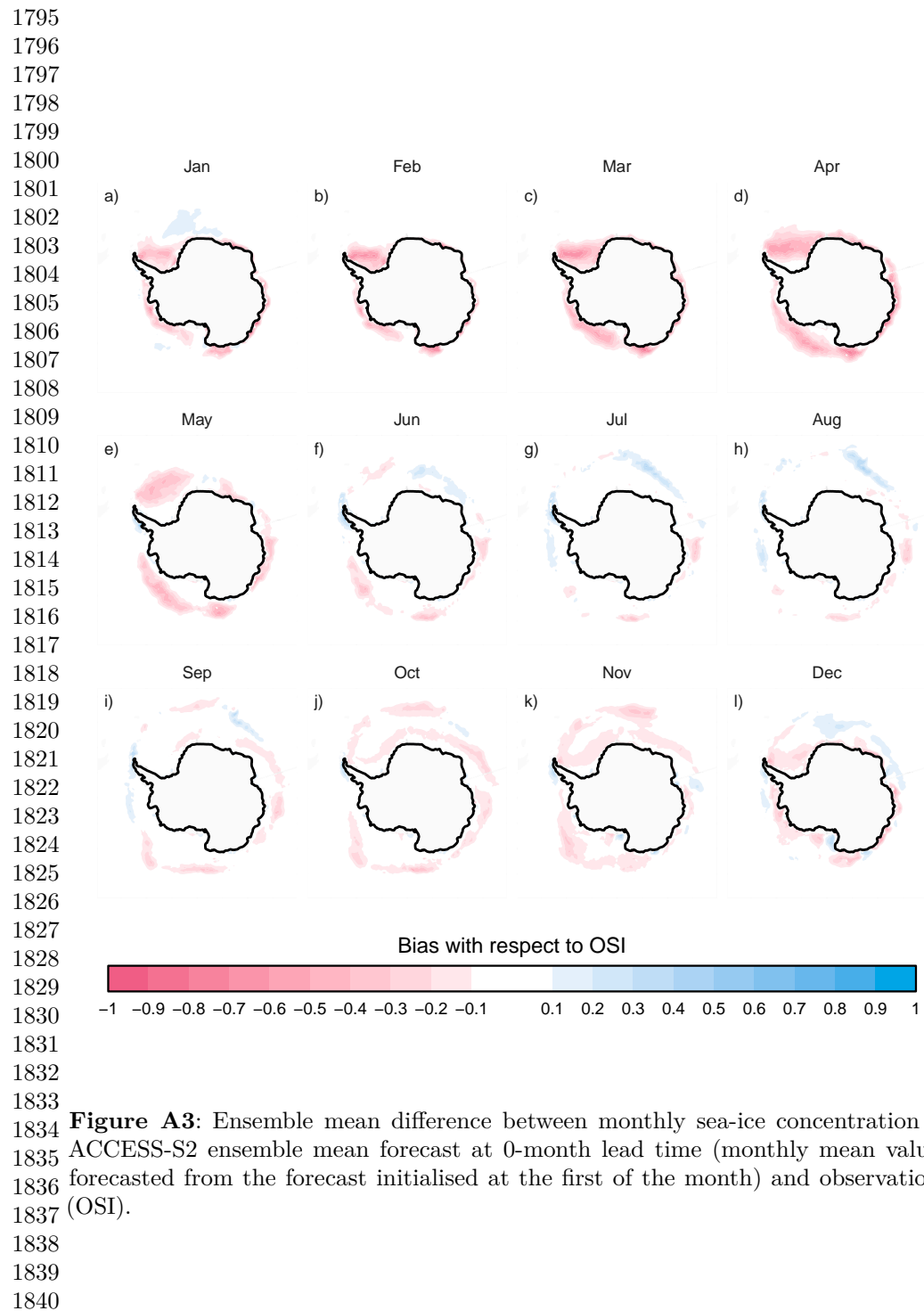


Figure A2: Mean daily sea-ice extent growth ($10^6 \text{ km}^2/\text{day}$) in ACCESS-S1 (green) and ACCESS-S2 (purple) hindcasts and observations (black), computed as the mean daily differences in sea-ice extent between each date and the next for each forecast month. Values are smoothed with a 11-day running mean.



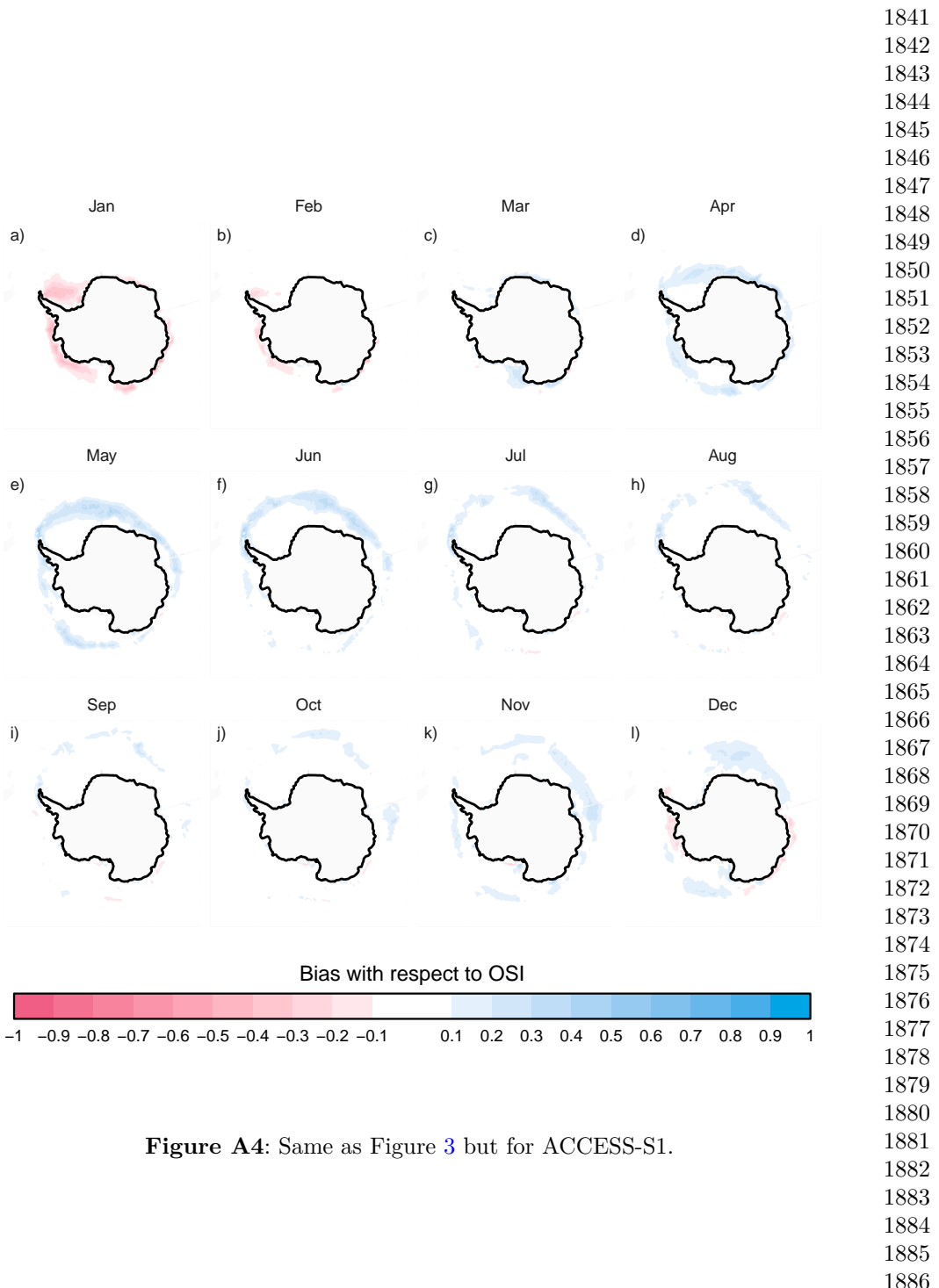


Figure A4: Same as Figure 3 but for ACCESS-S1.

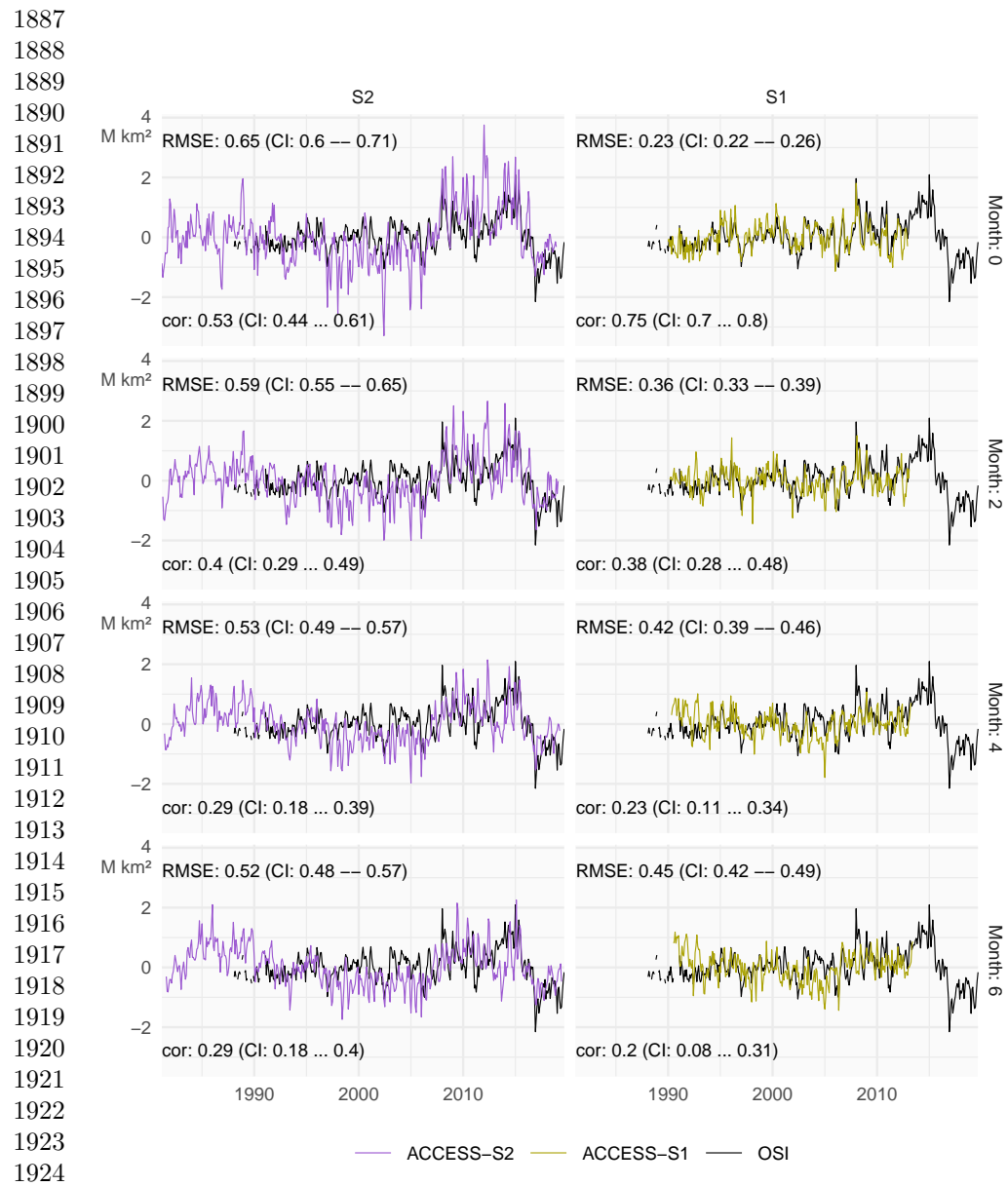


Figure A5: Monthly mean sea-ice extent anomalies of the observations (black) and forecasts from ACCESS-S1 (right column; purple) and ACCESS-S2 (left column; green) at lead times of 0, 2, 4, and 6 months. The RMSE and correlation during the overlapping period of ACCESS-S1 and ACCESS-S2 hindcasts (1990–2013) are shown on the top left and bottom left of each panel respectively.

1930
1931
1932

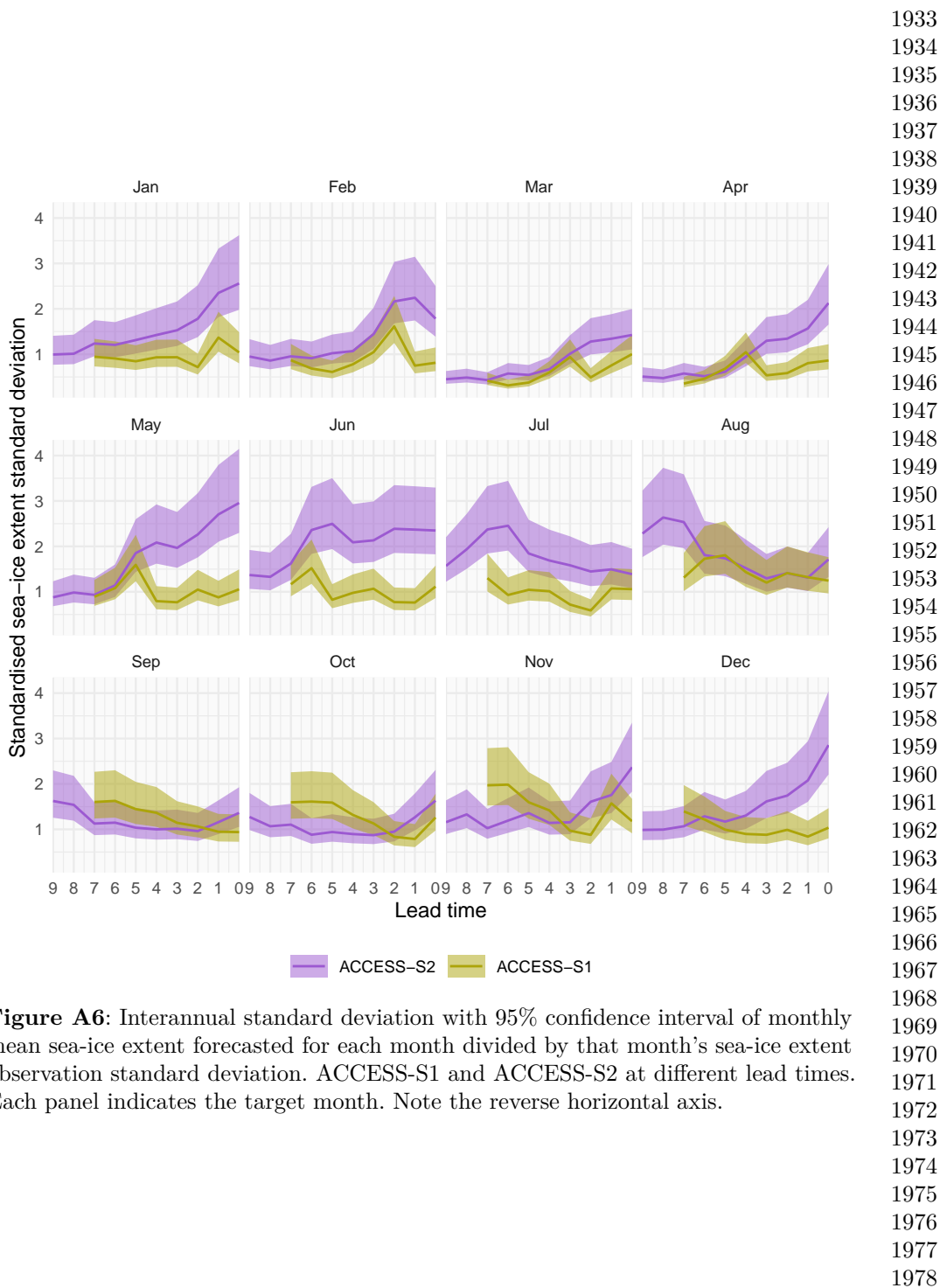
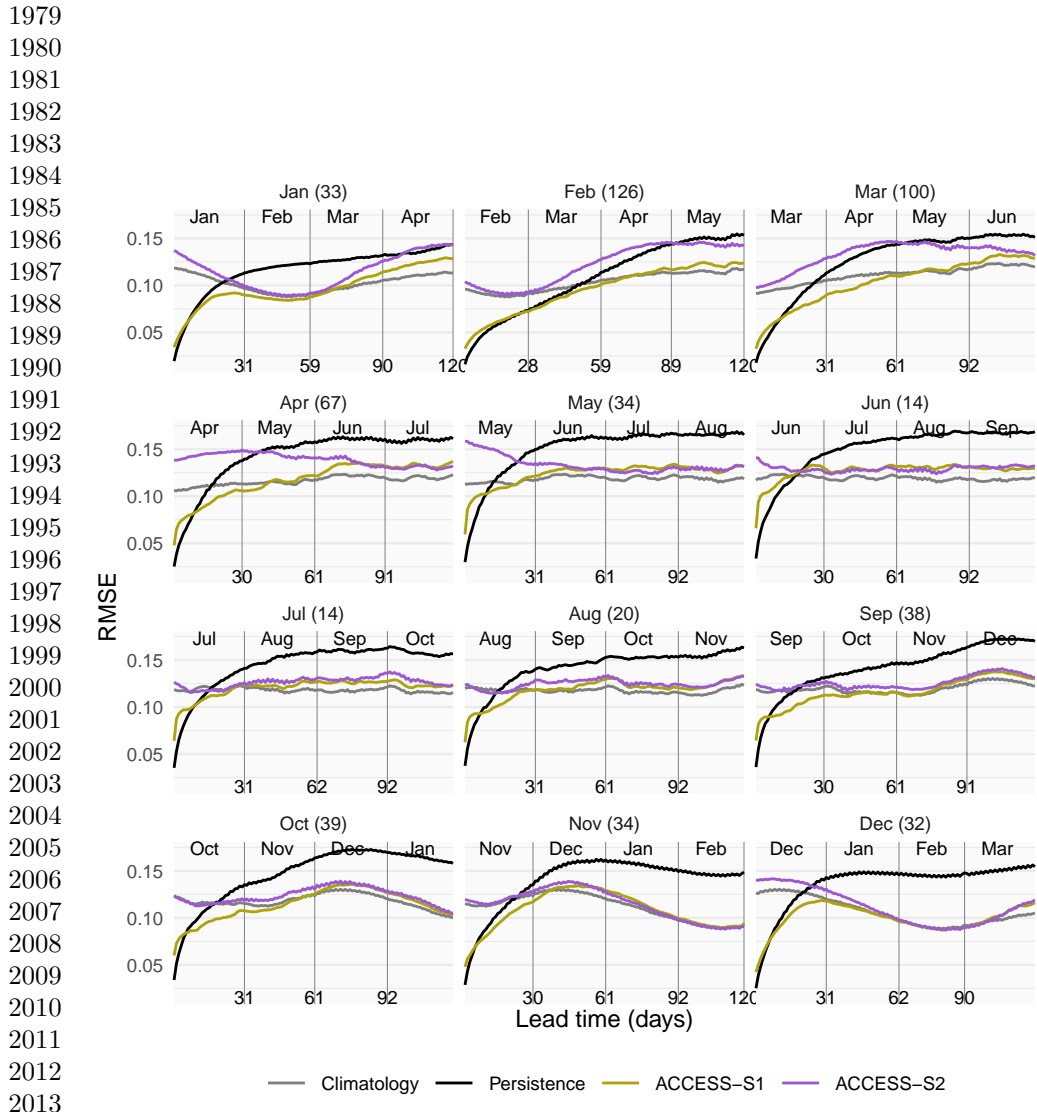


Figure A6: Interannual standard deviation with 95% confidence interval of monthly mean sea-ice extent forecasted for each month divided by that month's sea-ice extent observation standard deviation. ACCESS-S1 and ACCESS-S2 at different lead times. Each panel indicates the target month. Note the reverse horizontal axis.



2014 **Figure A7:** Mean RMSE of sea-ice concentration anomalies as a function of forecast lead time for all forecasts initialised on the first of each month compared with a 2016 reference forecast of persistence of anomalies (black) and climatology (gray). Only the 2017 first 120 days are shown. In parentheses, the shortest time at which ACCESS-S1 and 2018 ACCESS-S2 mean RMSE is not statistically different at the 99% confidence level.

2019
2020
2021
2022
2023
2024

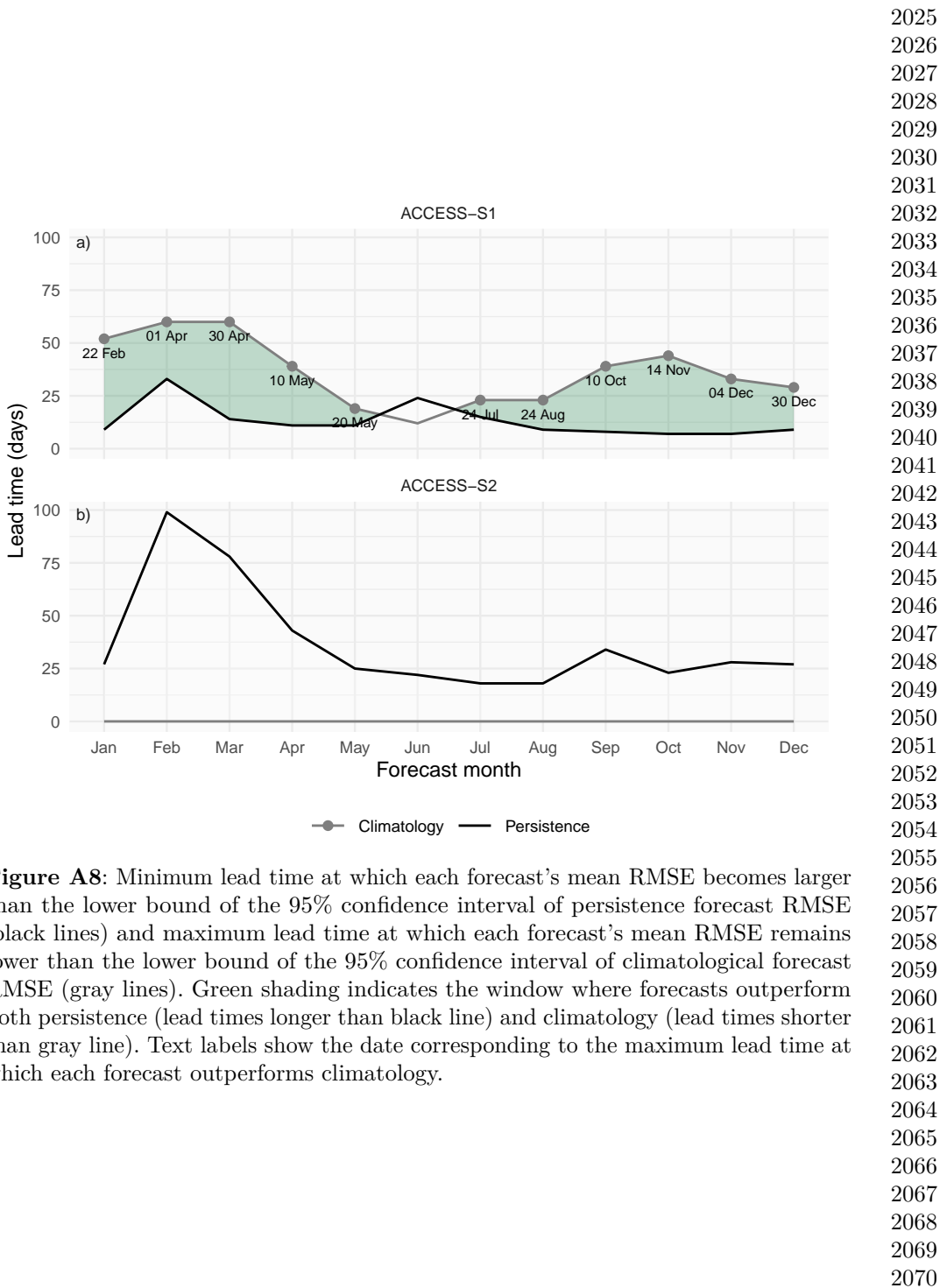
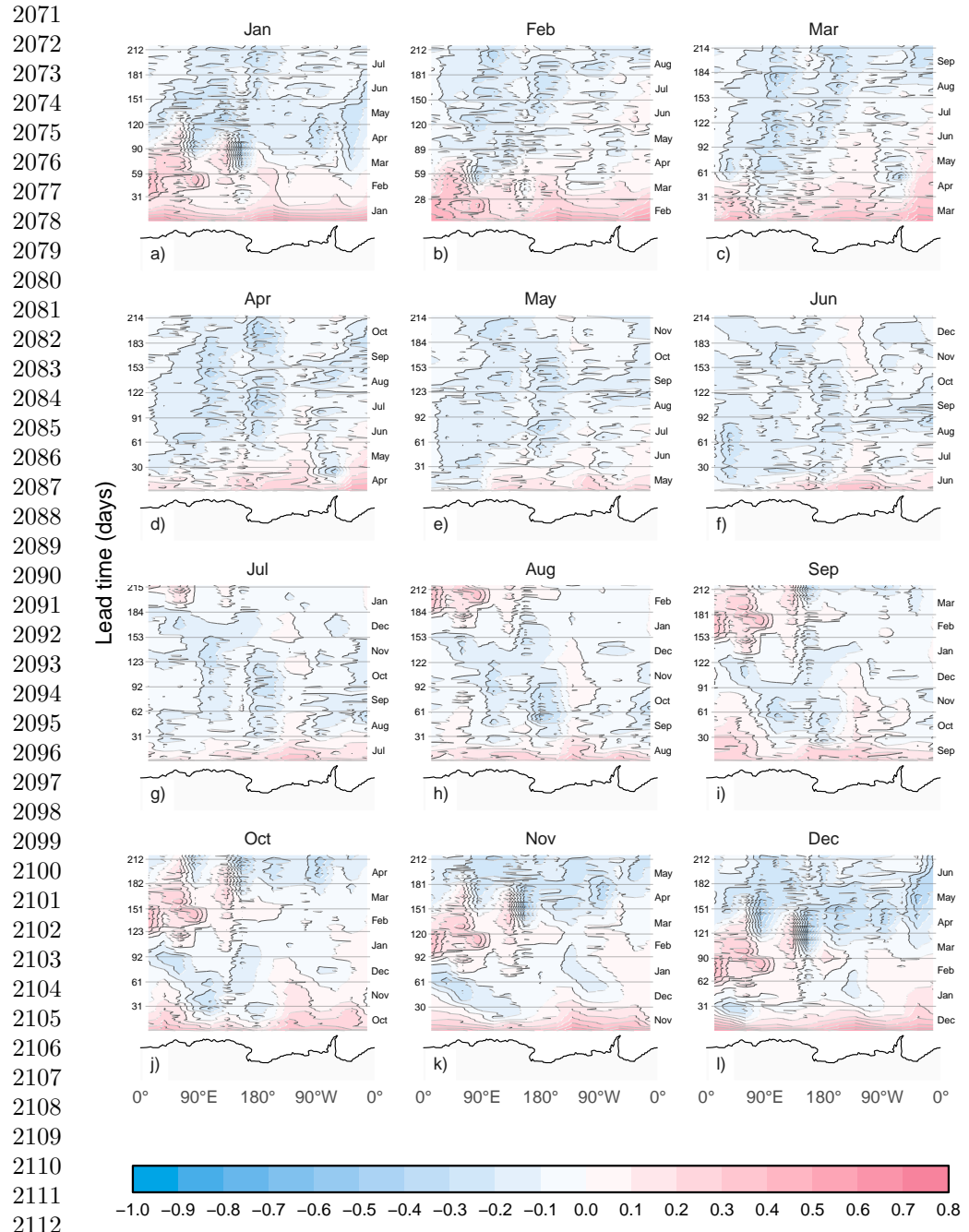


Figure A8: Minimum lead time at which each forecast's mean RMSE becomes larger than the lower bound of the 95% confidence interval of persistence forecast RMSE (black lines) and maximum lead time at which each forecast's mean RMSE remains lower than the lower bound of the 95% confidence interval of climatological forecast RMSE (gray lines). Green shading indicates the window where forecasts outperform both persistence (lead times longer than black line) and climatology (lead times shorter than gray line). Text labels show the date corresponding to the maximum lead time at which each forecast outperforms climatology.



2113 **Figure A9:** RMSE skill score of ACCESS-S1 forecasts with climatological forecast as
 2114 reference computed on 15 meridional slices 24° wide as a function of lead time and
 2115 longitude. Antarctica's coastline is shown at the bottom of each panel for reference.
 2116

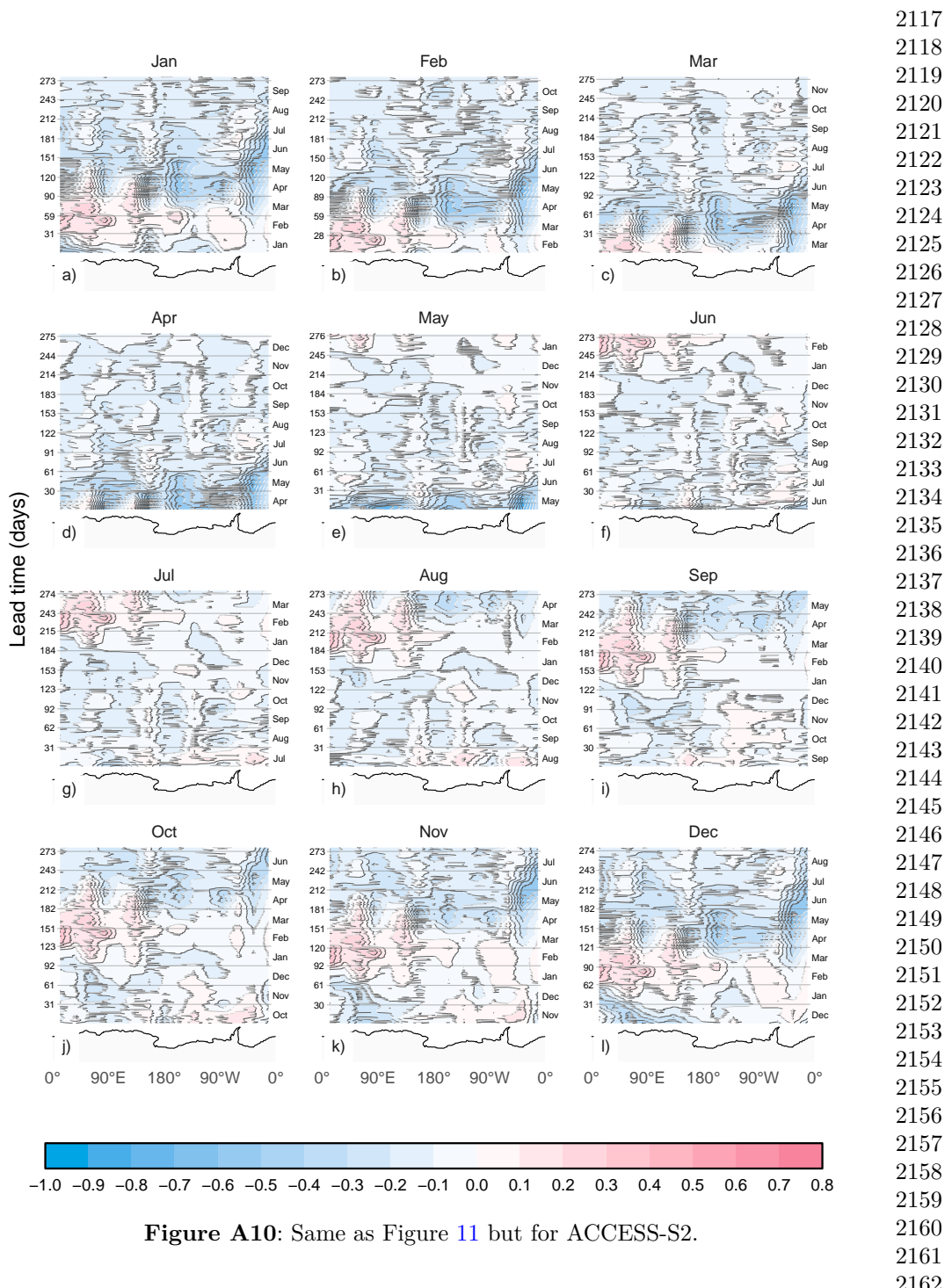
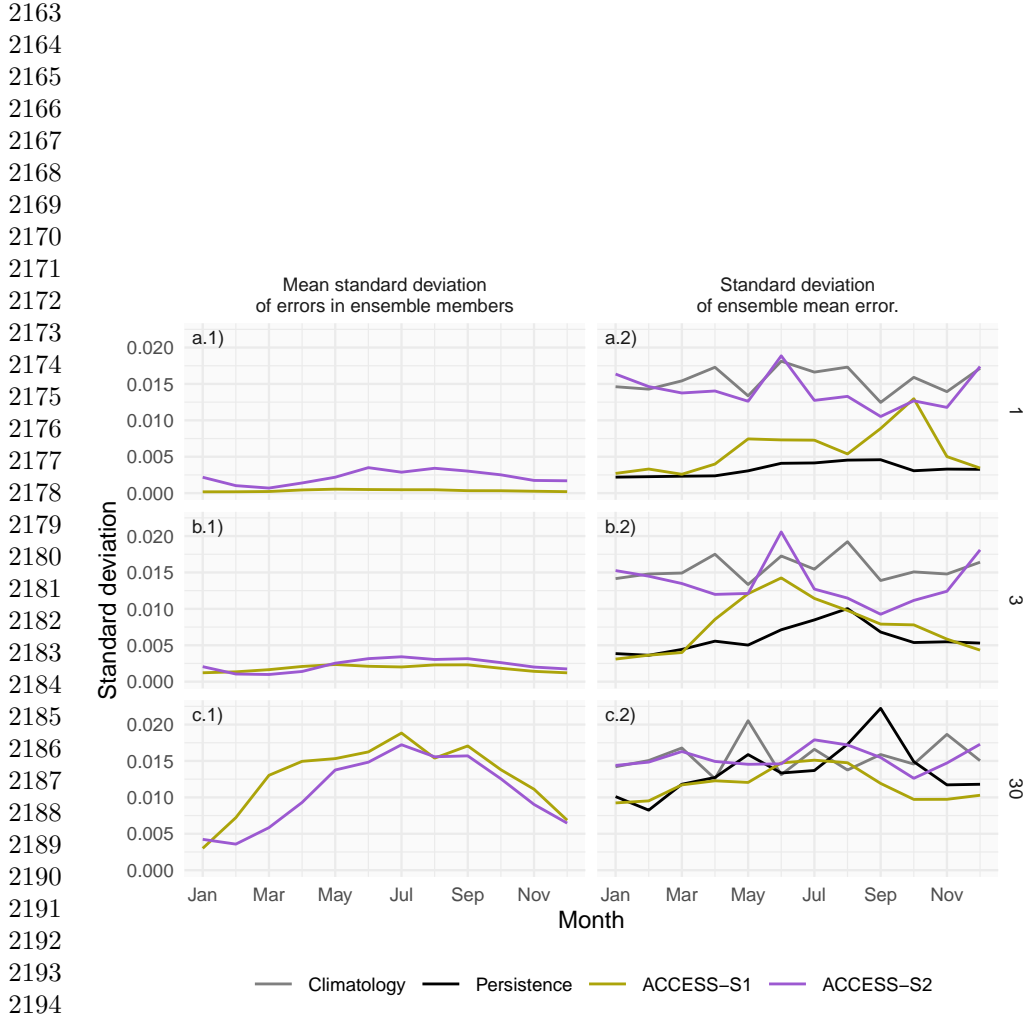


Figure A10: Same as Figure 11 but for ACCESS-S2.



2195 **Figure A11:** Decomposition of forecast error spread at 1, 5 and 30 days lead time for
 2196 ACCESS-S1 and ACCESS-S2 hindcasts across initialization months. The left column
 2197 shows the mean standard deviation of RMSE errors across ensemble members, while
 2198 the right column shows the standard deviation of the ensemble mean RMSE error and
 2199 the spread of the persistence and climatology forecasts errors.
 2200

2201
 2202
 2203
 2204
 2205
 2206
 2207
 2208